Tetrahedron 70 (2014) 517–532

Contents lists available at ScienceDirect

Tetrahedron

journal homepage: www.elsevier.com/locate/tet

Facile dearomatisation of porphyrins using palladium-catalysed hydrazination: the 5,15-diiminoporphodimethenes and their redox products

Louisa J. Esdaile [a], Grace L. Simpkins [a], Oliver B. Locos [a,†], Llew Rintoul [a], Martin P. Duriska [b,‡], Peter Turner [c], John C. McMurtrie [a], Dennis P. Arnold [a,*]

[a] School of Chemistry, Physics and Mechanical Engineering, Queensland University of Technology, GPO Box 2434, Brisbane 4001, Australia
[b] School of Chemistry, Monash University, Victoria 3800, Australia
[c] Crystal Structure Analysis Facility, School of Chemistry, University of Sydney, NSW 2006, Australia

ARTICLE INFO

Article history:
Received 18 August 2013
Received in revised form 21 October 2013
Accepted 4 November 2013
Available online 8 November 2013

Keywords:
Porphyrinoid
Diiminoporphodimethene
Crystal structure
Modelling
Density functional theory

ABSTRACT

The synthesis, electronic absorption and ^{1}H NMR spectra of a suite of novel porphyrinoids derived from *meso*-bromoporphyrins by palladium-catalysed aminations using ethyl and *tert*-butylcarbazates are reported. Instead of the expected carbazate-substituted porphyrins, a facile oxidative dearomatisation of the porphyrin ring occurs in high yield, especially for the nickel(II) complexes, resulting in high yields of 5,15-diiminoporphodimethenes (DIPDs). The analogous zinc(II) and free base DIPDs were also characterised, the former by X-ray crystallography. The oxidation and reduction reactions of DIPDs and their precursor carbazate porphyrins were studied. Density Functional Theory (DFT) was used to calculate the optimised geometries and frontier molecular orbitals of DIPD **Ni8c** and bis(azocarboxylate) **19c**, and Time Dependent DFT calculations allowed the prediction of electronic absorption spectra, whose characteristics corresponded well with those of the observed solution spectra. In the latter case, the calculated low-energy absorptions were unlike those of a typical porphyrin, due to the near-degeneracy of the highest filled frontier orbitals, and the wide energy separation between the unfilled orbitals. This feature was present in the observed spectrum.

1. Introduction

This work arose from our early attempts to prepare the then-unknown 'azoporphyrins', the porphyrin analogues of the azobenzenes. Anderson and co-workers predicted in 2002 that a diporphyrin covalently linked in the *meso*-position through an azo bridge would display strong conjugation between the macrocycle π-systems, conferring electronic properties different from those of the known ethene- and ethyne-linked dyads.[1] Subsequently, we reported the successful synthesis of the first azoporphyrins, and then expanded the range of these derivatives into functionalised versions, as well as an azo/butadiyne-linked tetrad.[2–4] It turned out that the oxidative homo-coupling of primary aminoporphyrins, such as **Ni1b** or **Zn1b** using catalytic copper(II) and air is a high-yielding route to azoporphyrins **Ni_2**/**$Zn_2$2**, provided that the opposite 15-*meso* carbon is substituted with, for example, a phenyl group (Scheme 1).[2] If the 15-position is unsubstituted, a remarkable head-to-tail coupling occurs, giving as the major products partially dearomatised systems, such as **3a** and **3b**.[2,5,6] Our original proposal to prepare the azoporphyrins, however, involved the Pd-catalysed coupling of alkoxycarbonyl-protected hydrazines (i.e., carbazates) with haloporphyrins, to be followed by deprotection, a second coupling, then a (presumed) facile dehydrogenative oxidation to the target **2** (Scheme 2). This multi-step route was based on the fact that typical pathways to azoporphyrins by diazonium coupling or partial reduction of nitrosoporphyrins had failed.[6]

Moreover, mild methods for the synthesis of azobenzenes have been reported using this strategy. In 1999, Bridger and co-workers synthesised *tert*-butoxycarbonyl (Boc)-protected aryl hydrazines using palladium catalysis.[7] Carbazates are ambidentate nucleophiles, and the amidation product predominated over the isomeric amination product. A Boc-protected aryl hydrazine dimer was formed as a side-product of the Pd-catalysed coupling of aryl bromides with *tert*-butyl carbazate. Cho and co-workers then reported

* Corresponding author. Tel.: +61 (0)7 3138 2482; e-mail address: d.arnold@qut.edu.au (D.P. Arnold).
† Present address: ChemCentre, Chemistry Precinct, Bentley, PO Box 1250, Perth 6152, Australia.
‡ Present address: Bruker Biosciences Pty Ltd, 1A/28 Albert St, Preston 3072, Australia.

0040-4020/$ – see front matter © 2013 Elsevier Ltd. All rights reserved.
http://dx.doi.org/10.1016/j.tet.2013.11.006

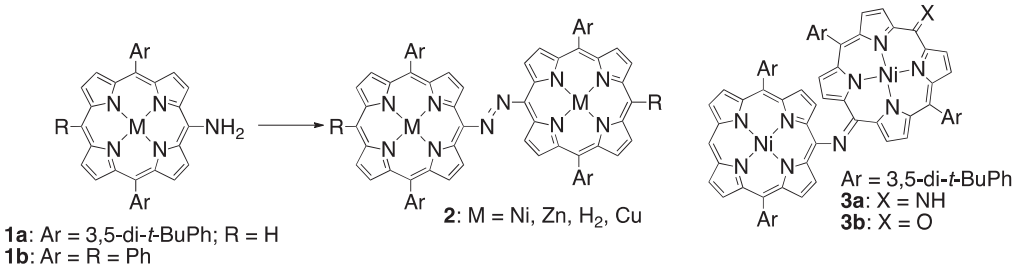

Scheme 1.

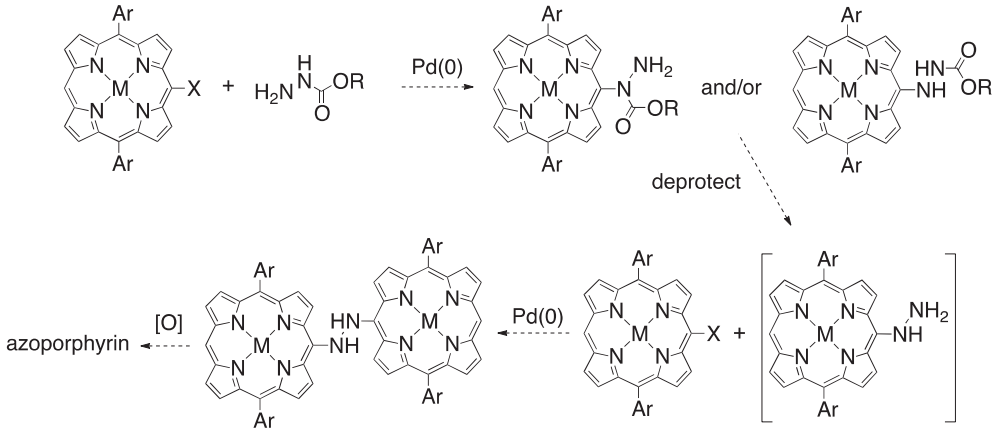

Scheme 2.

the synthesis of azobenzenes via the coupling of Boc-protected aryl hydrazines with aryl halides.[8] The reaction gave the azobenzene in a two-step procedure. The *N*′-Boc diarylhydrazines were synthesised using $Pd(OAc)_2$, P(*t*-Bu)$_3$ and Cs_2CO_3 in toluene at 110 °C in good to excellent yields with both electron-withdrawing groups and electron-donating groups attached. These were then directly oxidised to the corresponding azobenzenes with *N*-bromosuccinimide (NBS)/pyridine in dichloromethane (DCM) at room temperature.[8] Cho and co-workers then reported a copper mediated one-pot synthesis of azobenzenes from bis-Boc aryl hydrazines and aryl iodides.[9]

The amination and amidation of haloporphyrins has developed into a useful reaction for preparing a range of nitrogen-substituted porphyrinoids (NSPs). Various amino- and amido-porphyrins, including both *meso*- and β-substituted cases, have been reported in recent years using metal catalysis, including the significant papers of Takanami et al.,[10] and Zhang and co-workers,[11] amongst several others.[12] In particular, this type of reaction has led to many examples of porphyrinyl tertiary amines being tested as dyes for solar cells.[13] Although an example of coupling of a carb*amate* was reported by Zhang's group,[11b] the carb*azates* have not been investigated by others. Herein, we report the details of our studies of the reactions of 5-bromoporphyrins and 5,15-dibromoporphyrins with carbazates under Pd-catalysis. Although we abandoned this route to azoporphyrins because of our success with the copper-catalysed amine coupling, nevertheless this chemistry has uncovered the facile dearomatisation of the carbazate coupling products, which leads to the previously-unknown diiminoporphodimethene (DIPD) macrocycle **4**. Our early results were published in preliminary form in 2004,[14] and now we report all the synthetic details and our studies of the redox chemistry of this suite of carbazate-derived porphyrinoids. Moreover, we have performed Density Functional Theory (DFT) and Time Dependent DFT calculation on two candidate structures from the suite of compounds we prepared. We report their geometry optimisations, their predicted frontier orbital properties, and comparisons of experimental electronic absorption spectra with the predicted electronic transitions. From other recent results, the dearomatisation of certain *meso*-aminoporphyrins appears to be a more general reaction, which is leading to new lines of research.[15]

2. Results and discussion

2.1. Palladium-catalysed couplings of carbazates with nickel(II) *meso*-bromoporphyrins

As a starting point for this work, we chose 5-bromo-10,20-diphenylporphyrinatonickel(II) (5-bromoNiDPP) **Ni5** as the substrate. Its reaction with *tert*-butyl carbazate using the conditions of Takanami et al.[10] did not proceed cleanly to a mono-coupling product (Scheme 3).

TLC showed two products (or three from larger-scale reactions) were formed during this reaction and all were isolated. It was found that only products arising from attack by the *amino*-nitrogen of the carbazate were isolated from this reaction, and the possible amidation product, i.e., **6**, was not. The least polar compound was found to be the bright green mono-*meso*-substituted azocarboxylate **Ni7a**. The formation of the oxidised azocarboxylate product was unexpected, as the reaction conditions were thought to be reducing. These reactions were carried out in an argon atmosphere, and care was taken to exclude air from the reaction vessel. This result was promising, as it suggested that if hydrazine-linked porphyrin dimers could be prepared, they might spontaneously oxidise to give an azo-linked dimer.

This selectivity of the formation of the amino-product is presumably due to the steric crowding of the *meso*-position on the

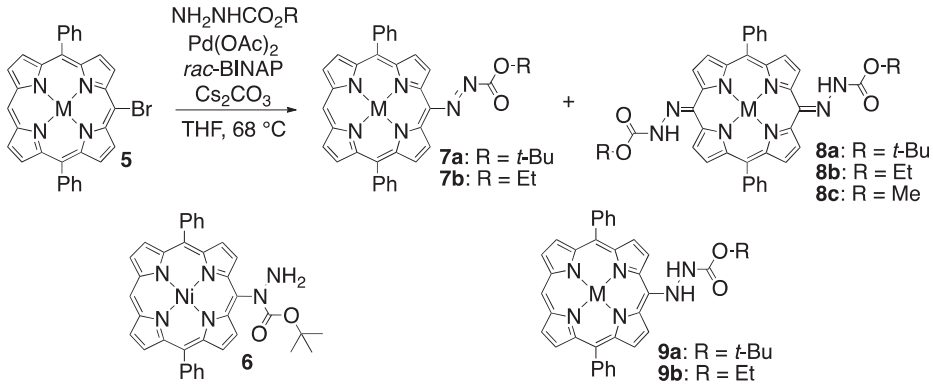

Scheme 3.

porphyrin macrocycle. Buchwald and co-workers found that amino- and amido-substituted products formed in equal amounts from *ortho*-substituted iodoarenes, whereas only the amido products formed from *para*-substituted iodoarenes.[16] The steric crowding of the *meso*-position of a porphyrin is comparable to that of an *ortho*-substituted iodoarene, and presumably the crowding of the *meso*-position and the use of the bulky 2,2′-bis(diphenylphosphino)-1,1′-binaphthyl (BINAP) ligand led to the selectivity of the formation of the terminal amino-substituted products.

More interestingly, the major product of this reaction was the unprecedented blue-green di-*meso*-substituted diiminoporphodimethene (DIPD) **Ni8a**, which was isolated in a crude yield of 72%. It was characterised using ^{1}H NMR, high resolution MS, UV/vis spectroscopy as well as X-ray crystallography, and was reported in our preliminary communication.[14] This product was very unexpected, as the starting material was mono-brominated and therefore only mono-*meso*-substituted products were envisaged. The loss of aromaticity also was a major surprise at that time, as a variety of mono- and di-aminated porphyrins had been synthesised previously, with no reports of porphodimethene products.[10,11] When the reaction of NiDPPBr with *tert*-butyl carbazate was repeated on a larger-scale, after the bromoporphyrin starting material was completely consumed, a minor red product was noted on the TLC plate, eluting between the two green compounds. Upon isolation, this red compound was found to be the mono-*meso*-substituted *carbazate* porphyrin **Ni9a**, characterised using ^{1}H NMR, high resolution MS, IR, UV/vis spectroscopy and elemental analysis. This compound was found to oxidise spontaneously to the azocarboxylate **Ni7a** upon exposure to air over a period of hours, and when exposed to acid was found to decompose to non-porphyrinic material.

We were able to prepare the carbazate porphyrin **Ni9a** selectively by reducing the reaction time from 25 h to 13 h. At 13 h the carbazate porphyrin was isolated in 84% recrystallised yield, even when a ten-fold excess of the carbazate was present. When the same ratios of starting materials were allowed to react for 24 h, the amount of **Ni9a** was reduced to 19%, and the yield of DIPD **Ni8a** increased from 5% to 54%. This increase in yield of the DIPD may be attributed to air seeping into the reaction vessel over the longer reaction time or during sampling for TLC analysis, despite our precautions. Moreover, the mono-*meso*-substituted azocarboxylate and carbazate porphyrins were then selectively synthesised from the coupling of 1 equiv of carbazate with a bromoporphyrin. Azocarboxylate **Ni7a** was synthesised in a 63% crude yield (25% recrystallised yield, due to the low-yielding recrystallisation) upon leaving the reaction mixture open to the air. However, the application of the oxidant 2,3-dichloro-5,6-dicyanobenzoquinone (DDQ) directly to the reaction mixture resulted in the decomposition of the porphyrin products.

To try to improve the ease of purification, separation and characterisation of the products obtained from the palladium-catalysed reactions, *tert-butyl* carbazate was replaced by *ethyl* carbazate. It was hoped that by replacing the *tert*-butyl group with an ethyl group, the solubility of the products in organic solvents might be lowered, thus improving the low-yielding recrystallisations. In addition, the ^{1}H NMR signal for the *tert*-butyl singlet of the DIPD resonated close to the signal for any water that was present in the solvent. This made the differentiation between similar compounds or the determination of the number of carbazate-type substituents on a compound difficult.

Ethyl carbazate was found to react within the same amount of time as the *tert*-butyl analogue, and gave the analogous three products: the azocarboxylate **Ni7b** and carbazate **Ni9b** and the DIPD **Ni8b**. It was found that the change in the group did result in easier separation by chromatography. This was due to the products' higher retention factors, so the requirement for a less polar solvent for the elution of the product meant that polar impurities no longer co-eluted with the DIPD product. However, it was found that changing to ethyl carbazate unfortunately did not significantly reduce the solubilities of the products.

To prepare the DIPD selectively, 5,15-dibromoporphyrin **Ni10** was subjected to the same conditions, using excess ethyl carbazate (Scheme 4). However, the yield for **Ni8b** was found to vary just as much when either the mono- or di-bromoporphyrin were employed, but the dibromoporphyrin was easier to purify, so it was henceforth used for the synthesis of DIPDs.

To synthesise the mono-substituted carbazate- and azocarboxylate porphyrins, 1 equiv of ethyl carbazate was combined with NiDPPBr. The carbazate porphyrin was either isolated or allowed to oxidise in air to the azocarboxylate. The azocarboxylate porphyrin **Ni7b** was isolated in up to a 63% yield using this method, and was characterised using ^{1}H NMR, MS, IR and UV/vis spectroscopy. The redox properties of these azocarboxylate and carbazate porphyrins, as well as those of the DIPDs, will be discussed in Section 2.3.

To avoid the dearomatisation reactions entirely, NiDPPBr **Ni5** was replaced by 5-bromo-10,15,20-*tri*phenylporphyrinatonickel(II) (NiTriPPBr, **11**). It was found that when 1 equiv of the carbazate was employed, the reaction proceeded sluggishly, and the products degraded over the longer reaction time required. When ten equivalents of carbazate were used, the reaction proceeded more rapidly (within 22 h) and upon allowing the reaction mixture to stir open to the atmosphere, the desired azocarboxylate **12b** was isolated in 67% crude yield (the carbazate porphyrin **13b** was not isolated under these work-up conditions). The azocarboxylate **12b** was characterised using ^{1}H NMR, high resolution MS and UV/vis

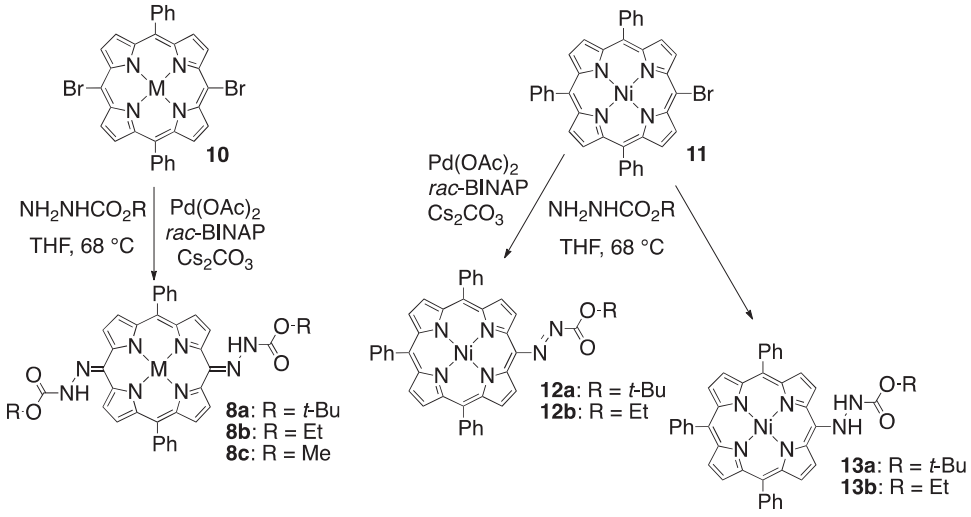

Scheme 4.

spectroscopy. In order to study the redox behaviour of this suite of compounds, we needed the carbazate porphyrin, and we found that it could be prepared in almost pure form by treating bromoporphyrin **11** with ten equivalents of *tert*-butyl carbazate in the presence of the standard palladium catalysts, but then isolating the products as rapidly as possible to avoid oxidation. The carbazate porphyrin **13a** was characterised using ^{1}H NMR, high resolution MS and UV/vis spectroscopy, and only 6% of the azocarboxylate **12a** was isolated under these conditions.

Thus the synthesis of the three major types of products formed from the coupling of alkyl carbazates with nickel *meso*-bromoporphyrins had been optimised to synthesise each product selectively. The broader applicability of these couplings was then studied using the zinc(II) and free base bromoporphyrins.

2.2. Palladium-catalysed couplings of carbazates with zinc(II) and free base *meso*-bromoporphyrins and the mechanism of the double coupling

The synthesis of the zinc(II) DIPD from 5,15-dibromo-10,20-diphenylporphyrinatozinc(II) **Zn10** was found to proceed cleanly to yield **Zn8b** in up to 82% recrystallised yield. DIPD **Zn8b** was characterised using ^{1}H NMR, high resolution MS, UV/vis spectroscopy and X-ray crystallography (see Section 2.4). The ruby-red zinc DIPDs were found to give the highest yielding recrystallisations of the series, as long as coordinating solvents (e.g., methanol or pyridine) were avoided during the recrystallisation. Unusually for most porphyrin synthetic research, the self-aggregation tendencies of Zn(II) porphyrinoids were actually advantageous in this series. Although the zinc complex did give the highest purified yield of all the DIPDs on one occasion, this preparation was found to be quite unreliable. On several occasions the reaction was repeated with no major products observed, and numerous side-products were isolated, which either degraded or were isolated in insufficient quantities to identify their structures. We do not have a satisfactory explanation for this lack of reproducibility.

To expand the variety of metals that could be coordinated to the DIPDs, the *free base* H_2DPPBr **$H_2$5** was coupled with excess *tert*-butyl carbazate (Scheme 3). The reaction yielded the dark orange free base DIPD **$H_2$8a** in a recrystallised yield of 37%, which was characterised using ^{1}H NMR, high resolution MS and UV/vis spectroscopy. It was found that the coupling with free base porphyrin was the most unreliable of the three that were trialled. The reaction was repeated on several occasions and the yields were difficult to reproduce. The repetition gave either no stable products or the desired DIPD highly contaminated and in low yields. The dibrominated starting material H_2DPPBr$_2$ **$H_2$10** was also subjected to the coupling reaction, in order to favour the formation of the DIPD product, and ethyl rather than *tert*-butyl carbazate was used to aid in the ease of separation. The desired product was formed only in low yield and the purification was not found to be any easier.

In order to synthesise the zinc and free base *mono*-substituted azocarboxylate and carbazate porphyrins, 1 equiv of ethyl carbazate was combined with either mono-brominated ZnDPPBr **Zn5** or H_2DPPBr **$H_2$5**. Remarkably, both of these reactions predominately resulted in the formation of the dearomatised DIPD products **Zn8b** and **$H_2$8b**, in low yields. This result is interesting, as these conditions were thought to be the most conducive to the formation of mono-substituted products. A large amount of unreacted starting material was also recovered, along with other side-products in trace amounts, which could not be characterised. It was concluded from these experiments that the nickel(II) porphyrins formed either mono- or di-substituted products, depending on the reaction conditions, whereas both the zinc and free base porphyrins formed the disubstituted DIPD products preferably, regardless of the conditions.

To avoid this reaction, the couplings with carbazates of a free base bromo substrate with a blocked 15-*meso* position, namely 5-bromo-15-phenyl-10,20-bis(3,5-di-*tert*-butylphenyl)porphyrin (H_2DAPPBr, **14**), was attempted (Scheme 5). In the only successful reactions, the catalyst Pd(dppe)$_2$ [dppe=1,2-bis(diphenyl phosphino)ethane] was used instead of the Pd(OAc)$_2$/BINAP system. The major product was the green azocarboxylate **15** (29%), but two other porphyrinoid free bases were also isolated, one blue and the other violet in solution. The ^{1}H NMR spectrum of the blue compound suggested strongly that it is the novel iminophlorin **16**. The details of the ^{1}H NMR spectroscopic results are presented in the Supplementary data. The violet compound appeared to be a tautomeric iminophlorin, presumably **17**, but its low yield precluded its full characterisation.

In summary, the synthesis of nickel DIPDs was the most reproducible and gave the highest crude yields, the zinc series was less repeatable but produced the highest recrystallised yields, and the free base was the lowest yielding and the least repeatable. Takanami et al. reported that nickel(II)-coordinated porphyrin starting materials resulted in the highest yields for amino- and

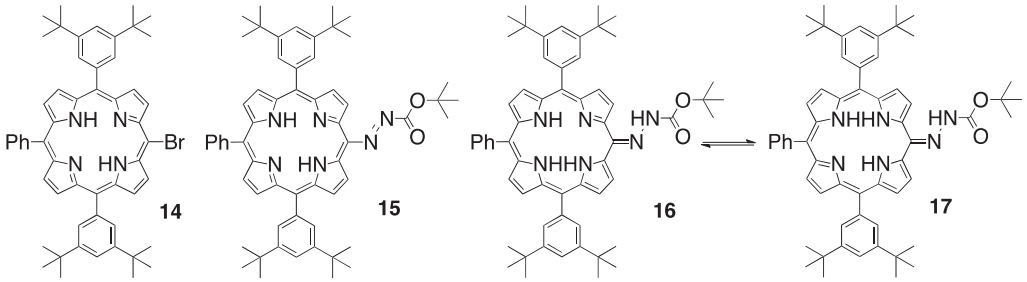

Scheme 5.

amido-porphyrins in Pd-catalysed couplings, followed by zinc(II), and finally free base, which was found to result in a complex mixture.[10] A similar result was also observed by Shen et al. for the nickel-catalysed amination of porphyrins.[12d] Thus for the *carbazate* nucleophiles reported here, our findings agree with those for the amines and amides reported by Takanami et al.[10]

Some control experiments were performed to try to understand better the formation of a disubstituted product from a mono-substituted starting material. The first experiment was to react unsubstituted H_2DPP **18** with excess *t*-butyl carbazate using the $Pd(OAc)_2$/*rac*-BINAP catalytic system. No change was observed after 25 h, the amount of time normally required for the full consumption of the brominated starting materials. Thus the bis-substitution requires the initial substitution to occur in order to allow the second carbazate molecule to attack the opposite free *meso*-position. excess carbazate, using the normal catalytic system. The reaction mixtures were monitored by TLC and it was found that both yielded the DIPD products, **Ni8a** and **Ni8b**, repectively. These mixtures were reacted for two weeks, and although the starting materials were not entirely consumed, no more product was being formed in either mixture, and side-products were starting to form. During these experiments, we observed by TLC that both the mono-azocarboxylate and carbazate porphyrins were found in both reaction mixtures. These results did not clarify, which of the azocarboxylate and carbazate porphyrins lead to the formation of the DIPDs. However, the azocarboxylate porphyrin **Ni7a** was found to give the DIPD product in a higher yield (47%) and with fewer side-products than the carbazate porphyrin **Ni9b** (20%). This observation led us to propose a mechanism for the formation of the diimino-porphodimethenes, which is shown in Scheme 6. This mechanism

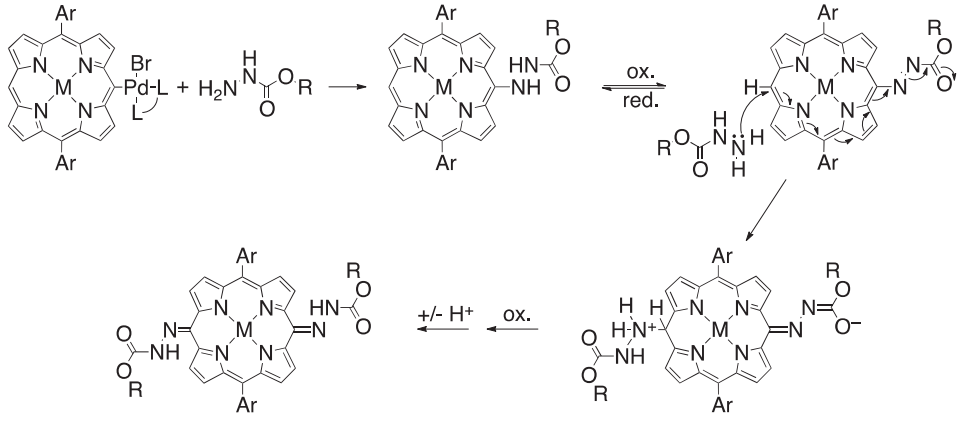

Scheme 6.

The synthesis of the DIPD product was then trialled from the coupling of $NiDPPBr_2$ **Ni10** with excess ethyl carbazate in the *absence* of both palladium and ligand, to see if a simple nucleophilic substitution reaction was responsible. The starting material was completely consumed after *four weeks*, however the long reaction time meant that many side-products also formed. The DIPD product **Ni8b** was indeed isolated, but only in <10% crude yield. The DIPD **Ni8b** was also isolated from the coupling of a ten-fold excess of ethyl carbazate with **Ni10**, in the presence of base and $Pd(OAc)_2$ only (i.e., ligand-free). The starting material had been consumed within 18 h, and **Ni8b** was isolated in a 14% crude yield.

In order to investigate another pathway to the DIPDs, mono-*meso*-substituted azocarboxylate **Ni7a**, and mono-*meso*-substituted carbazate porphyrin **Ni9b** were separately treated with requires that after the formation of the carbazate porphyrin, the latter is oxidised (perhaps due to the oxygen in the solvent, as the solvent was not degassed for these reactions) to the azocarboxylate porphyrin. The electron-withdrawing azocarboxylate group then activates the opposite, unsubstituted *meso*-position, allowing the nucleophilic attack of a second carbazate. This results in a phlorin-type intermediate with one exocyclic imine bond, analogous to the species **16**/**17** possibly prepared from H_2DAPPBr, which is then oxidised to give the stable DIPD. There have been some recent examples of formal nucleophilic substitution of hydrogen by *N*-nucleophiles, including some in the absence of any metal catalysts.[17] So the reactions in this scheme have precedents, and it is clear that strongly electron-withdrawing substituents, such as azocarboxylate encourage this reaction.

2.3. Redox reactions of the carbazate coupling products

The study of the redox properties of the bis(carbazate) porphyrins and their metal complexes is rather complicated, due to the tendency of these compounds to oxidise partially to the DIPDs. We thought that the oxidation of a DIPD might proceed rather simply to a bis(azocarboxylate). However, the reduction of a bis(azocarboxylate) could result in either the bis(carbazate) porphyrin or the DIPD. The result of the reduction could of course be a mixture of the two products, which would be difficult to separate. Therefore, we chose to examine first the mono-*meso*-substituted carbazate porphyrin. The oxidation of the carbazate porphyrin **Ni13a** should result in the corresponding azocarboxylate **Ni12a** and the reduction of **Ni12a** should re-form **Ni13a**. In fact, the oxidation of **Ni13a** proceeded as expected to give the **Ni12a** in a 95% recrystallised yield. Upon the addition of 1 equiv of the oxidant DDQ, the reaction proceeded rapidly, with an immediate colour change from red to green.

To test the reductive process, **Ni12a** was treated with $NaBH_4$ in THF/methanol at room temperature and the mixture was monitored by TLC. After stirring the mixture at room temperature for 40 min, the **Ni12a** had converted to the carbazate **Ni13a** quantitatively. To check the stability of the carbazate, the mixture was then heated to reflux and the carbazate porphyrin slowly began to convert to the primary amine **Ni1b** and to the *meso*-unsubstituted NiTriPP. The mixture was then refluxed overnight, after which the carbazate was fully consumed and the major product was found to be NiTriPP, isolated in 48% yield. A small amount of the impure aminoporphyrin **Ni1b** was also isolated. The cleavage to the aminoporphyrin and the complete loss of the nitrogen substituent are rather difficult to explain, and deserve further investigation. We reported in 2006 the amination of NiTriPPBr to **Ni1b** using unsubstituted hydrazine as the nucleophilic coupling partner, so N–N cleavage is perhaps not unexpected, but reductive cleavage of the primary amino group from a porphyrin has not been previously reported.[18] Harper observed, however that in the $NaBH_4$/Pd/C reduction of the free base nitroporphyrin $H_2TriPPNO_2$ to $H_2TriPPNH_2$, if the reaction is not quenched within 10 min, extensive over-reduction to H_2TriPP becomes a problem.[19] In the analogous 5,10-diarylporphyrin series, Bašić used very short reaction times to avoid this reaction.[20] Although it is hard to imagine an actual synthetic use for this reaction, it is a possible method for clean removal of an NH_2 or NO_2 substituent from a *meso*-position.

Turning now to the disubstituted series, DIPD **Ni8b** was treated with an excess of DDQ, and an instantaneous colour change was observed (Scheme 7). The mixture changed from the blue-green of the DIPD to the bright green of the azocarboxylate. The fully aromatic bis(azocarboxylate) **19b** was isolated in 71% recrystallised yield and was characterised by ^1H NMR, MS, IR, UV/vis spectroscopy and elemental analysis. The *tert*-butyl DIPD **Ni8a** was also oxidised in this manner and gave the *tert*-butyl bis(azocarboxylate) **19a** in a lower yield of 36%, due to difficulties in recrystallisation. We also tried this oxidation with iodine in DCM and silver(I) in the form of $AgPF_6$ and $AgOCOCF_3$ in DCM, but little or no conversion was observed.

The reverse process, reduction of the bis(azocarboxylate) **19b** was then attempted, by treatment with a ten-fold excess of $NaBH_4$ (5 equiv per azocarboxylate moiety). After stirring at room temperature for 15 min, the azocarboxylate was fully consumed, and the major product was the DIPD **Ni8b**, while a minor polar product was also observed by TLC. The mixture was stirred at room temperature for 1 day and then refluxed for 1 day, as no further reduction appeared to be occurring at the lower temperature. Upon separation of the resulting mixture, it was found that **Ni8b** remained as the only porphyrinic material, and it was isolated in a 59% crude yield. It is interesting to note that the fully reduced bis(carbazate) was not observed in this reaction, which shows the remarkable stability of the DIPDs. In the monofunctionalised series, the carbazate/azocarboxylate redox pair can be reliably interconverted, while in the bis series, the DIPD/azocarboxylate pair can be realised from both sides, but the bis(carbazate) is elusive.

2.4. X-ray crystal structure of the zinc(II) 5,15-diiminoporphodimethene Zn8b

It should be noted that we have drawn the relative stereochemistry about the two C=N double bonds in the DIPDs as giving the whole molecule C_2 symmetry (as a planar projection). Only one isomer was ever observed in the ^1H NMR spectra of **Ni8a** and **Zn8b**, for example, and the crystal structure we reported in our preliminary communication, namely Ni(II) complex **Ni8a**, indeed exhibited this disposition of the substituents.[14] The exocyclic imine bonds have C=N bond lengths of 1.299 and 1.297 Å, whereas the N_{imino}–N_{amido} bonds both have bond length of 1.349 Å. The average bond lengths of the dipyrromethane units are similar to those in a fully conjugated porphyrin, with a mean bond length of 1.38(9) Å, with the exception of those flanking the imine bond. The average C_{meso}–C_α bond length for the carbons adjacent to the imine bond was found to be 1.45(4) Å. This increase, in the vicinity of 0.06(5) Å, has previously been reported for the dioxoporphyrins and the porphodimethenes.[21,22] There exists strong out-of-plane distortion of the macrocycle, similar to that previously reported for other nickel porphodimethenes.[23] This distortion is illustrated as a linear display in Fig. 1. This shows that there is a small amount of saddle-type distortion on the β-carbons labelled C_3 and C_{13} (where the imino-substituents are attached to C_{10} and C_{20}). The average Ni–N_4 distance was found to be 1.891 Å, which allows the central nickel

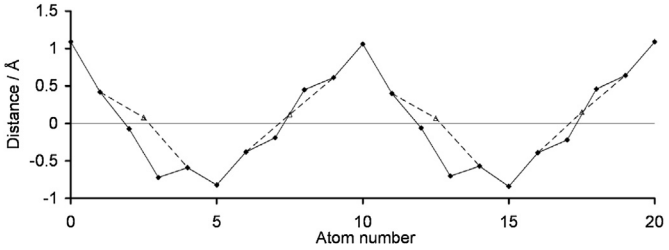

Fig. 1. Displacements (Å) of atoms from the mean $C_{20}N_4$ plane in crystals of nickel(II) diiminoporphodimethene **Ni8a**. The X-ray crystal structure was reported in Ref. 14.

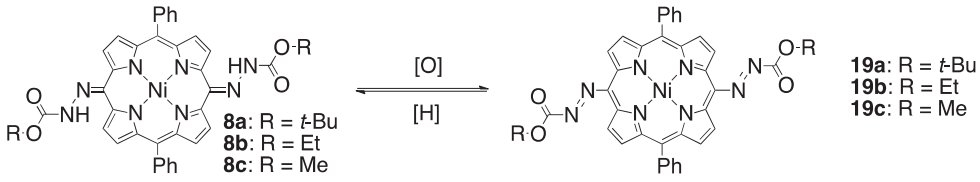

Scheme 7.

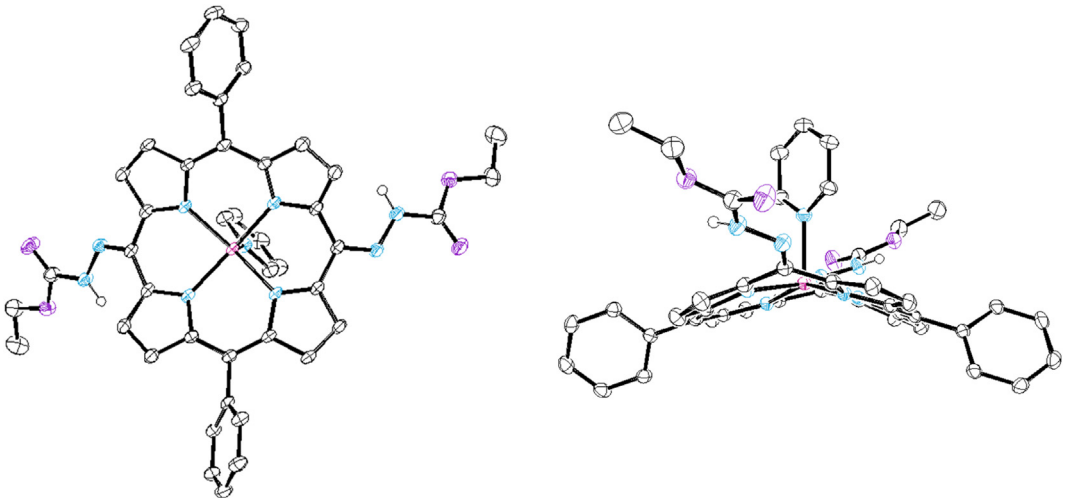

Fig. 2. Structure of zinc(II) diiminoporphodimethene **Zn8b** determined by single-crystal X-ray analysis. Disordered water and dioxane solvent molecules are omitted for clarity.

atom to have almost exact square planar geometry. Osuka and co-workers reported similar Ni–N_4 bond lengths for their quinodimethene product.[22]

Single crystals of the Zn(II) analogue **Zn8b** that were suitable for crystallographic analysis were grown from the slow diffusion of water into a solution in dioxane and pyridine. In the crystal structure, the metal ion is coordinated in N_4 core of the porphyrin, with a molecule of pyridine also coordinated to the zinc to give a five-coordinate complex with approximate square-based pyramidal geometry. The crystals also contain one dioxane and two water molecules for each complex giving the crystal formula [**Zn8b**(pyridine)]·dioxane·$2H_2O$. Face-on and edge-on views of the structure are shown in Fig. 2. The complex has crystallographic C_2 symmetry (C_2 axis passes through the zinc atom and is coincident with the Zn–$N_{pyridine}$ bond). The C_{meso}=N_{imino} bond lengths of 1.303(2) Å and the N_{imino}–N_{amino} bond lengths are 1.368(2) Å. The average bond lengths of the dipyrromethene units were 1.39(3) Å, again with the exception of the carbons adjacent to the imine carbon, with an average length of 1.46(8) Å, the difference being similar to the nickel analogue. The central zinc atom projects from the $C_{20}N_4$ mean plane by 0.61 Å, and the average Zn–N_4 distance is 2.07(8) Å. The Zn–$N_{pyridine}$ bond length was found to be 2.085(2) Å, which is shorter than those in simple porphyrins (2.14–2.20 Å)[24] and those found by Senge and Smith for the dioxoporphyrins (2.12–2.13 Å),[22] and approximately equal to the 2.084 Å reported for a tetracyanoporphodimethene **20**.[21] Shorter Zn–$N_{pyridine}$ bond lengths have been attributed to stronger pyridine coordination due to the higher positive charge on the core of the macrocycle.[21]

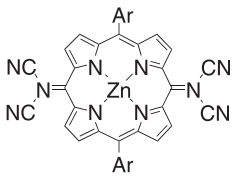

20: Ar = 3,5-di-*t*-BuPh

A linear display of the out-of-plane distortion is displayed in Fig. 3, which shows that the macrocycle displays a hybrid distortion between ruffled and saddled. The maximum out-of-plane distortion is on the β-pyrrolic C_3 and C_{13}. This deformation may be attributed to a twist of the phenyl ring towards the distorted β-carbon, the C_6 mean plane of the phenyl ring lying at a 61.2° angle from the $C_{20}N_4$ mean plane. Anderson's zinc(II) tetracyanoporphodimethene had a severely non-planar saddle shape, which was attributed to the steric repulsion between the β-hydrogens and the nitrile substituents.[21] To compare further the degree of modification of the porphyrin macrocycle geometry with a similarly dearomatised compound, Fig. 4 shows the bond distances and out-of-plane distortions of our DIPD **Zn8b** and porphodimethene **20**.

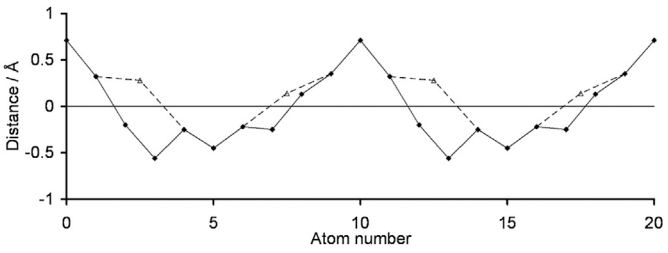

Fig. 3. Displacements (Å) of atoms from the mean $C_{20}N_4$ plane in crystals of zinc(II) diiminoporphodimethene **Zn8b**.

2.5. Spectroscopic properties of the 5,15-diiminoporphodimethenes

2.5.1. Electronic absorption spectra. To examine the effect of the carbazate substituent, the absorption spectrum of the carbazate porphyrin **13a** was compared to that of unsubstituted NiTriPP. The lone pairs of the nitrogen substituents are expected to influence the electronic spectrum of the carbazate porphyrin. Fig. 5 shows that NiTriPP possesses a Soret band with a maximum at 409 nm, whereas **13a** has its maximum at 422 nm. The Q-bands of NiTriPP are found at 522 and 549 nm, whereas for **13a** they are located at 489, 535 and 576 (shoulder) nm, indicating a significant electronic effect of the substituent. The lowest-energy Q-band for the primary amine **Ni1b** lies at 599 nm. Its structural and chemical properties indicate there is a strong overlap of the N lone pair with the porphyrin electrons,[18] so the more modest red-shift occasioned by the carbazate group clearly shows less interaction between macrocycle and substituent.

Once oxidised to the mono-azocarboxylate **12a**, the resulting effects on the absorption spectrum—a dramatic red-shifting of the Soret and the Q-bands—can be attributed as an extension of the porphyrin conjugation due to the azo group. The Soret band shifts to 446 nm and the Q-band to 616 nm, a remarkable red-shift

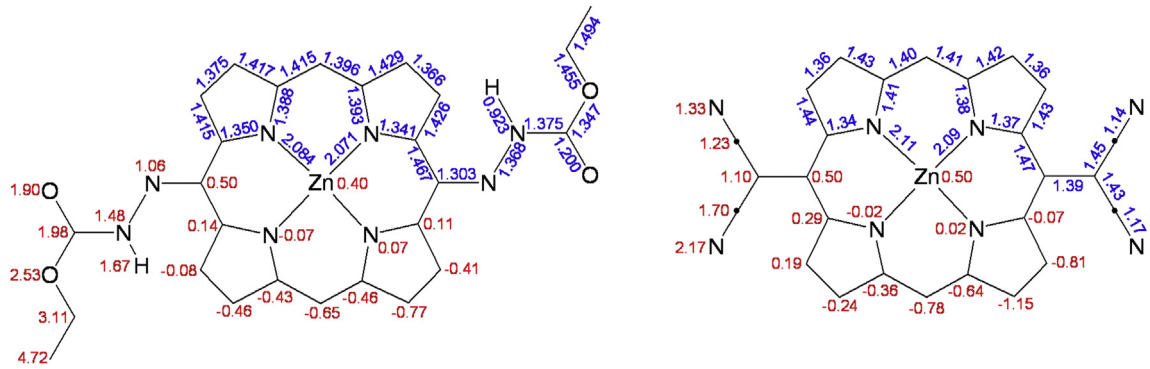

Fig. 4. Comparisons of the molecular dimensions (in blue) and out-of-plane atom displacements (red) for **Zn8b** (left) and the tetracyanoporphodimethene complex **20** (right) reported by Blake et al.[21]

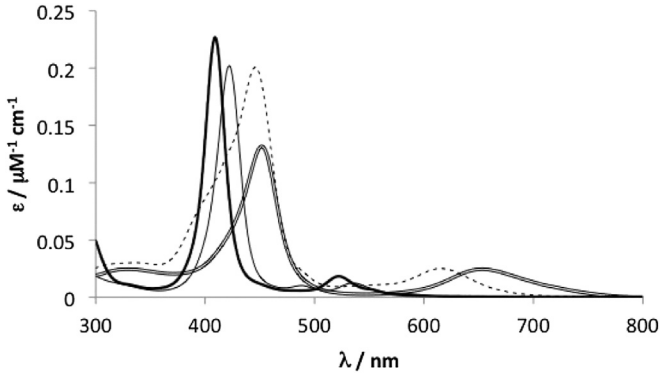

Fig. 5. Electronic absorption spectra (in dichloromethane) of NiTriPP (bold solid line), nickel(II) carbazate **13a** (solid line), nickel(II) mono(azocarboxylate) **12a** (dashed line) and bis(azocarboxylate) **19b** (double line).

compared with **13a**. While the Soret band of the azocarboxylate maintains its intensity, relative to the carbazate porphyrin, it has broadened significantly and the Q-bands of the azocarboxylate have doubled in intensity, relative to the Soret band (Fig. 5). Anderson noted similar electronic properties in the *meso*-arylazo-substituted porphyrins, the only comparable examples in the literature.[1] The broadening and red-shifting of the bands were more dramatic for the latter compounds, however, as they were further conjugated to aryl groups.

In order to examine the electronic effects when either one or two azocarboxylate groups are substituted on a porphyrin, the spectrum of bis(azocarboxylate) **19b** is also shown in Fig. 5. The effect of the second azocarboxylate group is to increase the intensity of the Q-bands in relation to the Soret band, and to red-shift both the Soret and Q-bands. The Soret exhibits only a minor shift from 446 nm to 452 nm (a 300 cm^{-1} shift), while the Q-bands have a greater shift from 616 nm to 653 nm (920 cm^{-1}). The Q-band of **19b** is also very broad. The theoretical calculations described in Section 2.6 shed some light on this unusual spectrum. The azocarboxylate substituent apparently possesses a similar electronic influence to the nitro group, for which a Q-band red-shift from 5-nitro- to 5,15-dinitroNiDPP of 562–583 nm (640 cm^{-1}) is found; however the second nitro group has a more profound effect on the Soret band, with a 980 cm^{-1} shift (from 408 to 425 nm) observed.[25]

The UV/vis spectrum of the DIPD **Ni8a** is shown below in Fig. 6, together with the zinc and free base analogues **Zn8b** and **$H_2$8a**. The Soret band is reduced and the Q-bands have increased in relative intensity, as expected when the conjugation of a porphyrin is interrupted at opposite *meso*-positions, for example, **20**.[21] There is also a strong absorption centred at 334 nm, which has an extinction coefficient of approximately two-thirds of that of the Soret band. This absorption is not observed in typical porphodimethenes that lack the *N*-substituent. A nickel(II)OEP (H_2OEP=2,3,7,8,12,13,17,18-octaethylporphyrin) imino-oxo-porphodimethene was reported by Balch and co-workers to have an absorption band at 326 nm (as well as at 456, 536 and 660 nm),[26] whereas only two absorptions (445 and 556 nm) were reported for the zinc analogue.[27] The 5,15-dioxoporphyrins also display a relatively strong absorption in the region between 310 and 330 nm.[28] Most porphyrinoids, including porphodimethenes with exocyclic *C*=*C* bonds,[21,29] do display a weak absorption band in this region, however its intensity (both relative to the Soret band and absolute) is not usually as high.

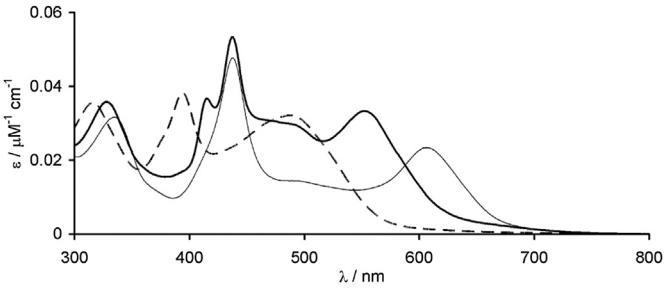

Fig. 6. Electronic absorption spectra (in dichloromethane) of nickel(II) diiminoporphodimethene **Ni8a** (bold solid line), zinc(II) diiminoporphodimethene **Zn8b** (solid line), and free base diiminoporphodimethene **$H_2$8a** (dashed line).

The UV/vis spectrum of the DIPD **Ni8a** shown in Fig. 6 can be compared with a fully oxidised bis(azocarboxylate) **19a** in Fig. 5 (the spectra were also compared in our communication).[14] This comparison dramatically illustrates the effect of the reduction in the conjugation of the porphyrin macrocycle, especially in the loss of intensity of the Soret band. Although the Q-bands have approximately the same intensity in both compounds, the Soret band of aromatised **19a** has regained the typical intensity of a normal porphyrin. The intensity of the band at 334 nm is also reduced once the macrocyclic aromaticity is restored, adding to the argument that this band should be attributed to the exocyclic imine bonds (see Section 2.6 below).

The spectra in Fig. 6 show that the zinc and free base DIPDs display blue-shifted spectra in comparison to the nickel analogue. The blue-shift is the most dramatic for the free base **$H_2$8a**, for which the Soret band is reduced in intensity as well. In fact the spectrum

of **$H_2$8a** is very different from even its Ni(II) analogue **Ni8a**, and so unlike a typical free base porphyrin, that is, it unrecognisable as such. This radical change in the spectrum is dramatic for a putative minor change of central substituent, but similar observations have been reported for the dioxoporphyrins. For example, the free base OEP dioxoporphyrin absorbs at 315, 408 and 492 nm, with extinction coefficient ratio 2.2:4.7:1.0,[28] whereas its Ni(II) complex absorbs very differently at 337, 458, 546 and 676 (weak) nm (7.7:23:4.3:1.0).[30] The Zn(II) analogue **Zn8b** is also unusual, having characteristics of both the others, but the absorption band attributed above to the exocyclic imine substituent is remarkably consistent for all three DIPDs. Modelling of the transitions by Density Functional Theory is described in Section 2.6.

2.5.2. The ^{1}H NMR spectra. The porphyrin regions of the ^{1}H NMR spectra of the *tert*-butylazocarboxylate and -carbazate porphyrins **Ni7a** and **Ni9a** are illustrated in Fig. 7. The effect of the electron-withdrawing azocarboxylate substituent can be seen in the broad spread of β-H peaks of >1 ppm. The most downfield β-H doublet, due to the 3- and 7-Hs, is remarkably shifted further downfield than the singlet *meso*-peak. This unusual peak inversion was not observed in the arylazo-substituted porphyrins, however it was observed in acetylene- and imine-linked porphyrin dimers.[1] Conversely, carbazate **Ni9a** possesses a broader doublet, resonating at 9.44 ppm, for the 3,7-β-protons adjacent to the carbazate substituent. The broadening may reflect rotational restriction of the bulky substituent. The 3,7-β-protons signal for the azocarboxylate **Ni7a** are much sharper, presumably due to the removal of the interfering N*H* atoms upon oxidation.

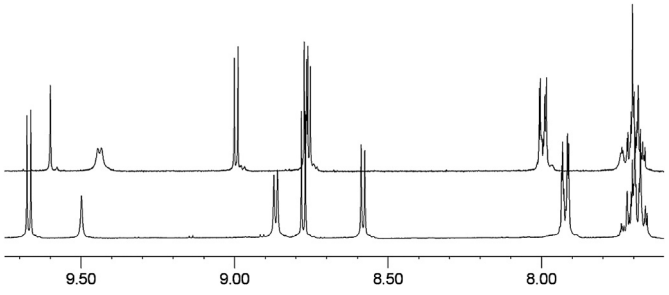

Fig. 7. Porphyrin proton region of the 400 MHz ^{1}H NMR spectra of nickel(II) mono(azocarboxylate) **Ni7a** (top spectrum) and nickel(II) carbazate **Ni9a** (bottom) in $CDCl_3$.

The triphenylporphyrin carbazate **13a** has a ^{1}H NMR spectrum typical of an unsymmetrically substituted 5,15-disubstituted porphyrin, and the NH signals were assigned as a result of the different rates of deuterium exchange with D_2O: a slightly broad peak at 7.67 ppm was found to disappear rapidly, so this peak was assigned as the amino N*H*, whereas the broader peak at 7.25 ppm took longer to diminish and was therefore assigned as the amido N*H* peak.

The ^{1}H NMR spectra of the mono- and bis(azocarboxylate)s (e.g., **Ni7b**, **19b**) make an interesting comparison (Fig. 8). The spectrum **19b** is typical for a symmetrically substituted NiDPP. The β-peaks occupy a smaller range and the most downfield β-peak is upfield, compared with that of **Ni7b**, despite the presence of two strongly electron-withdrawing groups. As also suggested by the electronic spectra (Fig. 5) and the DFT calculations (section 2.6 below), this reflects the reduction in the aromaticity/ring current of this strongly axially-asymmetric porphyrin. Remarkably, this effect is also manifest in an upfield shift of the signals for the *ortho*-protons of the 10,20-phenyl groups. Because of the complete elimination of the macrocyclic ring current, the β-protons of the nickel DIPD **Ni8b** are shifted substantially upfield when compared to its oxidation product **19b**. The β-protons of the DIPD appear as four sharp doublets between 6 and 7 ppm (Fig. 8).

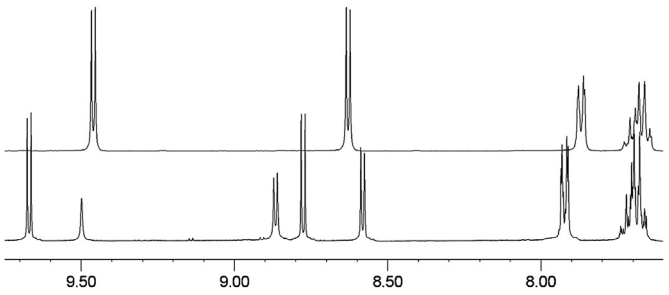

Fig. 8. Porphyrin proton region of the 400 MHz ^{1}H NMR spectra of nickel(II) bis(azocarboxylate) **19b** (top spectrum) and nickel(II) mono(azocarboxylate) **Ni7b** (bottom) in $CDCl_3$.

Porphodimethenes and dioxoporphyrins naturally also show this effect.[5,29,31] The amido protons give rise to the slightly broader singlet at 8.78 ppm, which was confirmed using D_2O exchange. We initially thought that DIPDs might exhibit only one pair of doublets arising from the β-protons, depending on the rate of inversion of the imino nitrogens. The 2D-NOESY experiment revealed cross-peaks between only one of the β-peaks (at 6.85 ppm) and the N*H* peak. This indicates that, on the ^{1}H NMR timescale, the amido proton lies in closer proximity to one side of the macrocycle than the other, rather than lying orthogonal to the macrocycle, and implies a slow rate of inversion of the imino nitrogens. Thus in solution the average structure has C_2 symmetry, which is more or less maintained in the solid state (Section 2.4).

The zinc DIPD **Zn8b** has a ^{1}H NMR spectrum very similar to that of the nickel analogue **Ni8b**, and the spectrum of the free base **$H_2$8b** is also similar in the pyrrole proton region. Notably, the inner N*H* protons resonate at 12.42 ppm, whereas in an aromatic free base porphyrin their signals are typically located at approximately −3 ppm. In the absence of macrocyclic conjugation, these protons resemble those of simple pyrroles. This effect has also been noted for porphodimethenes and dioxoporphyrins.[21,29,32,33] Two of the signals for the β-pyrrole protons in the spectra of **$H_2$8a** and **$H_2$8b** are broader than the others; this is due to small couplings to the pyrrolic NH in the same ring. As the macrocycle is no longer aromatic, the inner NHs are not undergoing tautomerism, allowing observation of this coupling. When **$H_2$8a** was treated with D_2O, not only does the signal at 12.42 ppm disappear, but the coupling is lost, and all four β-pyrrole signals appear as sharp doublets (Supplementary data, pages S7, S8).

2.6. Density Functional Theory modelling of nickel(II) 5,15-diiminoporphodimethene and its oxidation product

Because of the unique nature of the DIPDs, and the fact that we had the solid state structures in hand, it seemed worthwhile to attempt to model the new macrocyclic system using Density Functional Theory (DFT) calculations, and to see whether the calculations could predict the geometry and the electronic absorption spectrum. To this end, the model structures **Ni8c** and **19c** were subjected to theoretical calculations using the DFT model. Electronic structure and time-dependent calculations were subsequently performed on the resulting optimised geometries using the same parameters. The comprehensive results for both compounds are provided in the Supplementary data of the optimised geometries, the frontier molecular orbital surfaces (HOMO−1, HOMO, LUMO, LUMO+1), and tables of the most intense excited state transitions in the visible to near-IR regions.

The optimised molecular geometry for **Ni8c** closely resembles that found in the solid state for **Ni8a**. The macrocycle is strongly ruffled, and the overall symmetry is close to C_2. The C_{meso}=N–NH–C(=O)–O–C moieties are almost planar, implying extensive 'amide resonance'. On the other hand, the optimised geometry for **19c** has C_1 symmetry, and the N=N units are disposed towards the same side of the macrocycle, yet the C=O units point away from each other. Other conformers were explored, and several lie in close energetic proximity. In the global minimum-energy conformer, one of the C_{meso}–N=N–C(=O)–O–C moieties is nearly planar, but the other has a torsion angle of 50° along the N=N–C=O unit. Notwithstanding this fact, the torsion angles C_α–C_{meso}–N=N, which are indicative of the delocalisation of the azo group with the porphyrin π system, are 24° for the substituent with the out-of-plane ester carbonyl, and 20° for the 'fully conjugated' substituent.

We carried out the TD-DFT transition modelling using the global minimum structure; the one-electron transitions for **Ni8c** are tabulated in the Supplementary data. As far as we know, this is the first report of the electronic structure calculations on a porphyrinoid like this with interrupted macrocyclic conjugation. The calculated gas-phase one-electron transitions are compared with the experimental spectra of the analogues **Ni8b** and **19b** measured in DCM in Fig. 9. As expected for a comparison of gas-phase with solution spectra, quantitative agreement is not observed, and also the calculated transitions are systematically higher in energy. This is often observed in TD-DFT calculations on mononuclear porphyrinoids using these methods.[34] Notably, three key features are reproduced by the calculations, namely (i) the red-shift when the aromaticity is restored in **19**; (ii) the broad asymmetric Q-bands of **19b** comprising three transitions with similar oscillator strengths at 670, 624 and 592 nm; and (iii) the increase in relative intensity of the Q-like band versus the Soret-like band for the DIPD, not unexpected for an interrupted porphyrinoid structure.

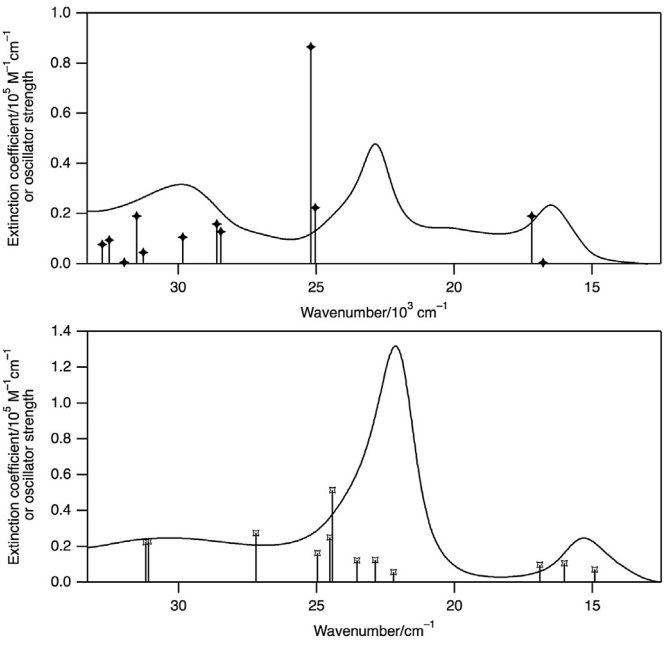

Fig. 9. Comparison of experimental absorption spectra in DCM (solid lines) with transitions calculated by TD-DFT in the gas-phase for **Ni8b**/**Ni8c** (top; vertical bars and filled markers) and **19b**/**19c** (bottom; vertical bars and unfilled markers).

The most interesting feature derived from the calculations is the multi-component Q-band of **19c**. The strong transverse electronic asymmetry across the 5,15-positions due to the conjugated azocarboxylate substituents results in the interesting situation of the HOMO−1 and HOMO being almost degenerate. The occupied frontier orbitals (deriving from the Gouterman orbitals of a D_{4h} metalloporphyrin) comprise the heavily modified 'a_{2u}-derived' HOMO−1 and the 'a_{1u}-derived' HOMO (Fig. 10), the former lying only 0.076 eV lower in energy. In contrast, the unoccupied frontier orbitals differ in energy by 0.86 eV, the LUMO having an interesting form. It has almost no electron density on the transverse 10,20-*meso* carbons, and large coefficients on the 5,15 carbons and the azo substituents, whereas the LUMO+1 has the opposite bias, but smaller coefficients on the azo groups.

When the transitions to electronically-excited states are examined (Table 1), an interesting pattern emerges. While the lowest-energy Q-band is mostly contributed (86%) by the HOMO–LUMO transition, the accompanying bands at 624 and 592 nm have a very mixed composition, as expected from the near-degeneracy of the occupied frontier orbitals. There are significant contributions from much deeper levels to the LUMO and LUMO+1. This situation is actually the reverse of the classical D_{4h} situation, for which the filled a_{2u}/a_{1u} HOMO−1/HOMO are close in energy, and the unfilled frontier orbitals are the e_g degenerate pair. This leads to the 'standard' situation described by Gouterman that explains the allowed/forbidden intensity pattern of the B and Q bands. In the present case with **19c**, the unusual large energy difference between the LUMO and LUMO+1 leads to the prediction of three 'Q bands' at 671, 624, and 592 nm. The 'Electron Density Difference Map' (EDDM), representing the difference between the electron distributions before and after the lowest-energy transition is shown in Fig. 11. The extent of charge transfer from the pyrrole rings of the core to the *meso* carbons and their attached electron-accepting substituents is dramatically illustrated in this plot.

Ni8b exhibits quite a broad tail on the red edge of the lowest-energy visible band, but there are no transitions with oscillator strength $f > 0.05$ predicted in this region for the optimised structure (Fig. 9, top). This feature, as well as the rather strong absorption in the 500 nm region, in which no significant transitions are calculated, may well be the result of populations of conformers rather different from the single one used in the TD-DFT calculations. Further discussions of these are unwarranted in the scope of this initial study.

3. Conclusion

The 5,15-diiminoporphodimethenes reported here are the first compounds of their type to be characterised. These porphyrinoids with reduced conjugation and exocyclic imino-bonds are closely-related to the oxoporphyrins and porphodimethenes. 'Interrupted porphyrins', such as these have interesting properties: oxoporphyrins are involved in the degradation of biological porphyrins, including the hemes, and 5,15-porphodimethenes, with their marked electronic asymmetry across the macrocycle, resemble the 5,15-dialkynylporphyrins, which exhibit non-linear optical properties. Quinoidal/cumulenic structures possessing porphodimethene character are thought to contribute to the excited states of the latter class of compound.[21]

As mentioned above, there are two reports of the closely-related 5-oxo-15-iminoporphodimethenes, namely the zinc and nickel OEP derivatives (H_2OEP=2,3,7,8,12,13,17,18-octaethylporphyrin). The former was reported by Fuhrhop and co-workers in 1970, and was prepared by treatment of 5-aminoZnOEP with Fe^{3+} salts in the presence of air.[27] This porphodimethene was found to hydrolyse easily to the dioxoporphyrin when left in chloroform or during chromatography. Fuhrhop rationalised the formation of this species as the oxidation of the aminoporphyrin to the radical-cation, which was stabilised by delocalisation from the amino N lone pair, forming an iminophlorin radical, which was then quenched by

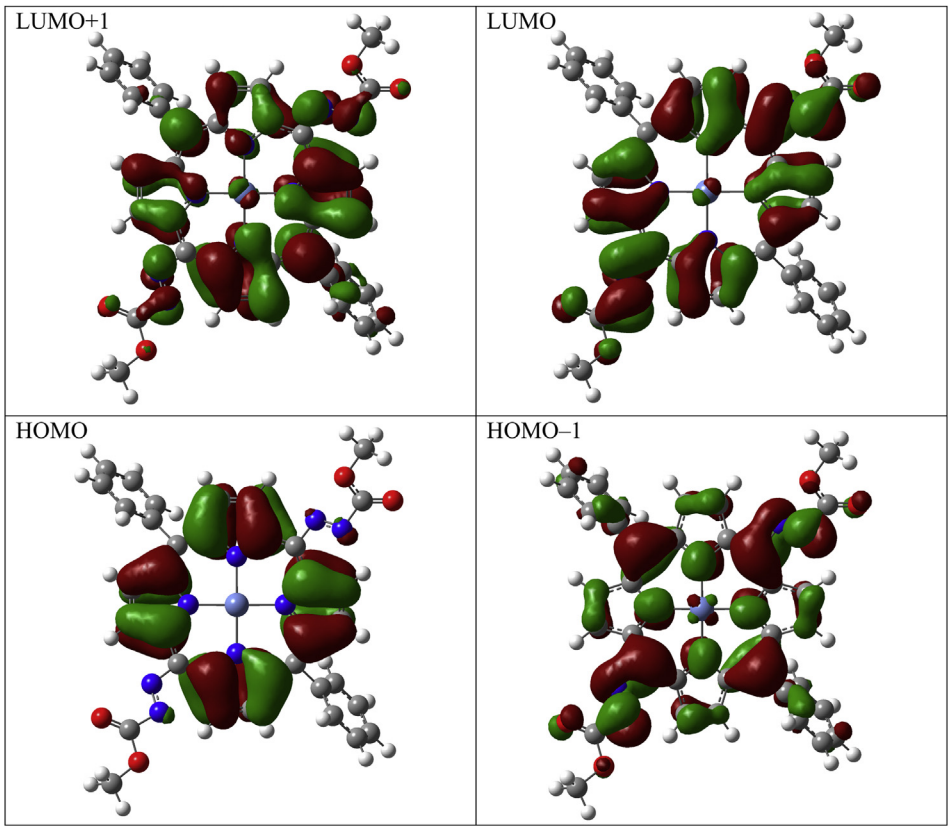

Fig. 10. DFT calculated frontier orbital surfaces for Ni bis(azocarboxylate) **19c**.

Table 1
One-electron excitations for Ni bis(azocarboxylate) **19c** calculated by TD-DFT (300–700 nm, $f \geq 0.01$, transition contribution ≥10%)

Excited state	Orbital composition				Excitation			Oscillator strength
					eV	nm	cm^{-1}	f
1	HOMO	→	LUMO	86	1.849	671	14,911	0.0712
2	HOMO−5	→	LUMO	34	1.986	624	16,016	0.1050
	HOMO−1	→	LUMO	43				
4	HOMO−5	→	LUMO	25	2.096	592	16,901	0.0974
	HOMO−2	→	LUMO	14				
	HOMO−1	→	LUMO	31				
	HOMO	→	LUMO+1	12				
11	HOMO−19	→	LUMO+3	18	2.754	450	22,213	0.0560
	HOMO	→	LUMO+1	15				
	HOMO	→	LUMO+2	39				
13	HOMO−7	→	LUMO	47	2.836	437	22,870	0.1241
	HOMO−1	→	LUMO+1	36				
16	HOMO−7	→	LUMO	19	2.918	425	23,532	0.1215
	HOMO−4	→	LUMO+1	33				
	HOMO−1	→	LUMO+1	32				
17	HOMO−3	→	LUMO+1	25	3.028	409	24,424	0.5140
	HOMO−1	→	LUMO	10				
	HOMO	→	LUMO+1	28				
	HOMO	→	LUMO+2	19				
18	HOMO−3	→	LUMO+1	59	3.040	408	24,522	0.2498
	HOMO	→	LUMO+1	14				
19	HOMO−1	→	LUMO+2	70	3.095	401	24,963	0.1629
27	HOMO−12	→	LUMO	35	3.371	368	27,192	0.2748
	HOMO−9	→	LUMO	12				
	HOMO−2	→	LUMO+2	20				
38	HOMO−13	→	LUMO	33	3.856	322	31,104	0.2276
	HOMO	→	LUMO+4	15				
39	HOMO−15	→	LUMO	5	3.868	321	31,195	0.2247
	HOMO−13	→	LUMO	13				
	HOMO	→	LUMO+4	47				

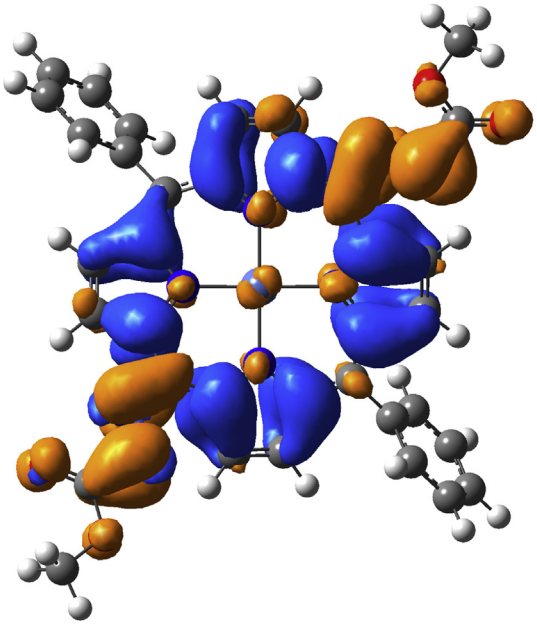

Fig. 11. Electron density difference map for the lowest-energy electronic transition (86% HOMO–LUMO) of **19c** calculated by TD-DFT. Blue: electron-poor region after transition; orange: electron-rich region after transition.

aerial oxygen.[27] More recently, Balch and co-workers synthesised the nickel analogue, by treatment of 5-aminoNiOEP with $FeCl_3$ in ethanol-stabilised chloroform.[26] The chemistry of porphyrinoids bearing double bonds at one or more *meso*-positions has been reviewed by Lee et al.[35]

The behaviour of alkyl carbazates in favouring the formation of DIPDs readily from the initial amination products is so far unique. We have tried other apparently similar nucleophiles in Pd-catalysed aminations of bromoporphyrins, with no success: tosylhydrazine, semicarbazide, thiosemicarbazide and 1,2-bis(ethoxycarbonyl)hydrazine. With hydrazine or 1,1-diphenylhydrazine, the N–N bond of the nucleophile is cleaved; in the former case, this led to the 1° aminoporphyrin, the 2° bis(porphyrinyl)amine, and the hydroxyporphyrin.[18] In the latter case, remarkably the only amino-product was the 2° amine.[36] Another interesting point is that there has so far been no mention of 5,15-bis(secondary amino)porphyrins undergoing dearomatisation to DIPDs: several authors have reported double aminations of 5,15-dihaloporphyrins,[11c,12a,12f] but no one has reported oxidation chemistry analogous to what we have found for the carbazates, even for 5,15-bis(4-methoxyanilino)porphyrin, which might be expected to be a prime candidate for such an oxidation.[12f] This contrasts with the facile dearomatisation found when aminoporphyrins undergo the head-to-tail oxidative coupling exemplified by structures **3a** and **3b**.[2,6] This type of dearomatisation has been reported to afford oligomeric analogues of **3a** under the appropriate conditions.[15]

In a subsequent report, we will describe the properties of the unique 5,10-diimino 'corner porphyrin' analogues and compare them with the present 5,15-disubstituted series.[37]

4. Experimental section

4.1. General

All solvents were Analytical Reagent grade, unless otherwise stated. Triethylamine (TEA) and pyridine were stored over KOH; toluene and diethyl ether were stored over freshly pressed sodium wire. The following solvents were freshly distilled prior to use (under argon): tetrahydrofuran (THF) from sodium wire and benzophenone; DCM, 1,2-dichloroethane (DCE) and MeCN from CaH_2; pyrrole was distilled without additives. Preparative column chromatography was performed on silica gel (40–63 μm), which was purchased from Qindao Haiyang Chemical Co. Ltd. China. Analytical TLC was performed on Merck Silica Gel 60 F_{254} TLC plates. The following porphyrin starting materials were prepared by literature procedures: H_2DPP,[38] H_2DPPBr,[25] H_2DPPBr$_2$,[39] NiDPPBr,[25] ZnDPP Br,[39] NiDPPBr$_2$,[25] ZnDPPBr$_2$,[39] H_2TriPP,[40] H_2TriPPBr,[41] NiTriPPBr,[41] H_2DAPPBr.[41]

^{1}H NMR experiments were recorded on a Bruker Avance 400 spectrometer at 400.155 MHz. All samples were recorded in $CDCl_3$ and 0.1% pyridine-d_5 was added to the solutions of zinc(II) porphyrins, unless otherwise stated. DQF COSY and gradient NOESY experiments were acquired using standard pulse sequences with 2048 points in f_2 dimension and 256 points in f_1 dimension. The gradient NOESY experiments were performed with a mixing time of 1.5 s. All coupling constants are recorded in Hertz. UV/Vis spectra were recorded on a Varian Cary 3 or Varian Cary 50 UV–visible spectrometer, and were recorded in DCM, unless otherwise stated.

Accurate Electrospray Ionisation (ESI) and Laser Desorption Ionisation (LDI) mass spectra were recorded at the School of Chemistry, Monash University, Melbourne. ESI measurements were performed using an Agilent 1100 Series LC attached to an Agilent G1969A LC-TOF system with reference mass correction using NaI clusters. An eluent of 50:50 DCM/MeOH with 0.1% formic acid was employed using a flow rate of 0.3 mL/min. Solvent aspiration was achieved by nitrogen gas flowing at 8 L/min. The source temperature was set to 350 °C and the capillary voltage to 4.0 kV. Liquid secondary ion mass spectrometry (LSIMS) mass spectra were recorded at the Organic Mass Spectrometry Facility, University of Tasmania, Hobart. LSIMS measurements were collected using *m*-nitrobenzyl alcohol as proton donor and CsI/TEG mixture for external reference, on a Kratos Concept ISQ double focussing Magnetic/Electrostatic Mass Spectrometer. IR spectra were collected using a Nicolet 870 Nexus Fourier Transform Infrared (FTIR) system equipped with a diamond internal reflection element. Samples for elemental microanalysis were dried at 80 °C under vacuum for 12 h and analyses were performed by the Microanalytical Service, School of Molecular and Microbial Sciences, The University of Queensland.

4.2. Palladium-catalysed reactions of carbazates and carbamates with *meso*-bromoporphyrins

Brominated porphyrin, amine or hydrazine source (0.5–10 equiv), $Pd(OAc)_2$ (7 mol %), *rac*-BINAP (20 mol %) and Cs_2CO_3 (7 equiv) were placed into a dry, argon-filled Schlenk flask and were dried under vacuum for 30 min. Freshly distilled, dry THF (5 cm^3 per 20 mg porphyrin) was added to the vessel and the reaction was stirred under argon at 68 °C. The reaction was monitored by TLC [DCM/*n*-hexane (1:1)] until the bromoporphyrin starting material was either fully consumed or perceived to be no longer being consumed. The reaction was quenched with water and stirred for 1 h open to air. The mixture was extracted into DCM, and the solvent was then removed by rotary evaporation. The products were separated using column chromatography. This procedure was utilised for the palladium-catalysed amination of porphyrins in all cases, unless otherwise stated.

*4.2.1. 5-(tert-Butoxycarbonylazo)-10,20-diphenylporphyrinatonickel (II) (**Ni7a**) and N,N′-bis(tert-butoxycarbonylamino)-5,15-diimino-10,20-diphenylporphodimethenatonickel(II) (**Ni8a**).* NiDPPBr (**Ni5**, 39.4 mg, 0.0668 mmol), *tert*-butyl carbazate (10 equiv, 88.6 mg, 0.668 mmol), $Pd(OAc)_2$ (1.0 mg, 0.0045 mmol), *rac*-BINAP (8.3 mg, 0.0013 mmol), Cs_2CO_3 (155 mg, 0.476 mmol) and dry THF (10 cm^3)

were stirred for 27 h at 68 °C. The products were separated using column chromatography [DCM then DCM/EtOAc (19:1)]. The first eluting compound after the orange starting material was the bright green **Ni7a** (15 mg, 35% crude yield), which resisted recrystallisation. The final product eluted upon the addition of MeOH and was the blue-green **Ni8a** (37 mg, 71% crude yield). DIPD **Ni8a** was recrystallised from a mixture of MeOH and H_2O (13 mg, 25%). **Ni7a**: ^{1}H NMR δ: 9.68 (2H, d, *J* 4.9, β H), 9.67 (1H, s, *meso* H), 8.99 (2H, d, *J* 4.9, β H), 8.83 (2H, d, *J* 4.9, β H), 8.67 (2H, d, *J* 4.6, β H), 7.98–7.96 (4H, m, phenyl H), 7.74–7.68 (6H, m, phenyl H), 1.81 (9H, s, CH_3); *m/z* (HRESI) 647.1706 ($[M+H]^+$, $C_{37}H_{28}N_6NiO_2$ calcd 646.1627); ν_{max} (cm^{-1}) 3330 (NH), 1740 (CO); UV/vis: λ_{max}/nm ($\varepsilon/10^3$ M^{-1} cm^{-1}) 334 (31.7), 437 (47.7), 536 (12.0), 606 (23.4). **Ni8a**: ^{1}H NMR δ: 8.72 (2H, br s, N H), 7.49–7.42 (10H, m, phenyl H), 6.96 (2H, d, *J* 4.6, β H), 6.85 (2H, d, *J* 4.2, β H), 6.69 (2H, d, *J* 4.9, β H), 6.68 (2H, d, *J* 4.4, β H), 1.47 (18H, s, CH_3); *m/z* (HRESI) 777.2439 ($[M+H]^+$, $C_{42}H_{38}N_8NiO_4$ calcd 776.2369); UV/vis: λ_{max}/nm ($\varepsilon/10^3$ M^{-1} cm^{-1}) 334 (31.7), 437 (47.7), 606 (23.4). Crystals were grown by the slow diffusion of water into a solution of **Ni8a** in dioxane. CCDC-268791 contains the crystallographic data for this compound.

*4.2.2. 5-[2-(tert-Butoxycarbonyl)hydrazo]-10,20-diphenylporphyrinatonickel(II) (**Ni9a**).* NiDPPBr (**Ni5**, 20.0 mg, 0.0334 mmol), *tert*-butyl carbazate (10 equiv, 111 mg, 0.836 mmol), $Pd(OAc)_2$ (1.3 mg, 0.0056 mmol), *rac*-BINAP (10.4 mg, 0.0167 mmol), Cs_2CO_3 (193 mg, 0.594 mmol) and dry THF (12.5 cm^3) were stirred for 13.5 h at 68 °C. The product was purified using column chromatography (DCM) and the red product **Ni9a** was recrystallised by the slow evaporation of DCM (46 mg, 84%). ^{1}H NMR δ: 9.60 (1H, s, *meso* H), 9.44 (2H, d, *J* 5.1, β H), 8.99 (2H, d, *J* 4.8, β H), 8.77 (2H, d, *J* 4.8, β H), 8.76 (2H, d, *J* 5.0, β H), 8.01–7.98 (4H, m, phenyl H), 7.74 (1H, br s, amine N H), 7.72–7.66 (6H, m, phenyl H), 7.17 (1H, br s, amide N H), 1.54 (9H, t, *J* 7.1, CH_3); *m/z* (LSIMS) 648.1788 (M^+, $C_{37}H_{30}N_6NiO_2$ calcd 648.1784); ν_{max} (cm^{-1}) 3354 (NH), 1718 (CO); UV/vis: λ_{max}/nm ($\varepsilon/10^3$ M^{-1} cm^{-1}) 415 (199.8), 528 (13.6), 582 sh. (3.0); Found: C, 68.27; H, 4.77; N, 12.81%; (Calcd C, 68.44; H, 4.66; N, 12.94).

*4.2.3. 5-(Ethoxycarbonylazo)-10,20-diphenylporphyrinatonickel(II) (**Ni7b**).* NiDPPBr (**Ni5**, 20.0 mg, 0.0334 mmol), ethyl carbazate (1 equiv, 3.5 mg, 0.0334 mmol), $Pd(OAc)_2$ (0.5 mg, 0.002 mmol), *rac*-BINAP (4.2 mg, 0.0067 mmol), Cs_2CO_3 (77.3 mg, 0.237 mmol) and dry THF (5 cm^3) were stirred for 18 h at 68 °C. The quenched reaction mixture was allowed to stir at room temperature, open to air, overnight. The product was purified using column chromatography (DCM, 13 mg, 63% crude yield) and the bright green **Ni7b** was recrystallised from THF/H_2O (5.2 mg, 25%). ^{1}H NMR δ: 9.67 (2H, d, *J* 5.1, β H), 9.50 (1H, s, *meso* H), 8.87 (2H, d, *J* 4.7, β H), 8.78 (2H, d, *J* 5.1, β H), 8.59 (2H, d, *J* 4.7, β H), 7.94–7.91 (4H, m, phenyl H), 7.70–7.68 (6H, m, phenyl *H*), 4.69 (2H, q, *J* 7.1, CH_2), 1.61 (3H, t, *J* 7.1, CH_3); *m/z* (MALDI-TOF-MS) 619.14 ($[M+H]^+$, $C_{35}H_{25}N_6NiO_2$ calcd 619.14); ν_{max} (cm^{-1}) 1733 (CO); UV/vis: λ_{max}/nm ($\varepsilon/10^3$ M^{-1} cm^{-1}) 443 (79.5), 534 (5.4), 612 (10.7).

*4.2.4. N,N′-Bis(ethoxycarbonylamino)-5,15-diimino-10,20-diphenylporphodimethenatonickel(II) (**Ni8b**).* $NiDPPBr_2$ (**Ni10**, 20.0 mg, 0.0295 mmol), ethyl carbazate (2.2 equiv, 6.75 mg, 0.065 mmol), $Pd(OAc)_2$ (0.5 mg, 0.002 mmol), *rac*-BINAP (3.7 mg, 0.0059 mmol), Cs_2CO_3 (68.2 mg, 0.209 mmol) and dry THF (5 cm^3) were stirred at 68 °C for 26 h. The product was purified using column chromatography [DCM then DCM/EtOAc (19:1)]. The resulting product **Ni8b** was dark green (13 mg, 61% crude yield) and was recrystallised from dioxane/H_2O at 4 °C. ^{1}H NMR δ: 8.80 (2H, br s, N H), 7.52–7.41 (10H, m, phenyl H), 6.96 (2H, d, *J* 4.9, β H), 6.84 (2H, d, *J* 4.4, β H), 6.71 (2H, d, *J* 4.9, β H), 6.68 (2H, d, *J* 4.4, β H), 4.33 (4H, q, *J* 7.1, CH_2), 1.34 (6H, t, *J* 7.1, CH_3); *m/z* (MALDI-TOF-MS) 721.15 ($[M+H]^+$, $C_{38}H_{31}N_8NiO_4$ calcd 721.18); ν_{max} (cm^{-1}) 3327 (NH), 1728 (CO); UV/vis: λ_{max}/nm ($\varepsilon/10^3$ M^{-1} cm^{-1}) 335 (33.4), 438 (48.7), 605 (23.0).

*4.2.5. N,N′-Bis(ethoxycarbonylamino)-5,15-diimino-10,20-diphenylporphodimethenatonickel(II) (**Ni8b**) synthesised without palladium.* $NiDPPBr_2$ (**Ni10**, 20.0 mg, 0.0295 mmol), ethyl carbazate (10 equiv, 30.7 mg, 0.295 mmol), Cs_2CO_3 (68.2 mg, 0.209 mmol) and dry THF (5 cm^3) were stirred at 68 °C for 4 weeks. The blue-green product was purified using column chromatography [DCM then DCM/MeOH (100:1)] and was isolated in 9% yield (1.9 mg).

*4.2.6. 5-(tert-Butoxycarbonylazo)-10,15,20-triphenylporphyrinatonickel(II) (**12a**) and 5-[2-(ethoxycarbonyl)hydrazo]-10,15,20-triphenylporphyrinatonickel(II) (**13a**).* NiTriPPBr (**11**, 50 mg, 0.074 mmol), *tert*-butyl carbazate (10 equiv, 101 mg, 0.74 mmol), $Pd(OAc)_2$ (1.3 mg, 0.006 mmol), *rac*-BINAP (9.3 mg, 0.015 mmol), Cs_2CO_3 (172 mg, 0.528 mmol) and dry THF (12.5 cm^3) were stirred for 17.5 h at 68 °C. The products were purified using column chromatography [DCM/*n*-hexane (1:1) then DCM]. The first eluting compound after the starting material was the bright green azocarboxylate **12a**, which was recrystallised by the evaporation of a DCM/pentane mixture (3.2 mg, 6%). The second major product eluted upon changing to DCM and was the red carbazate porphyrin **13a**, which was recrystallised by the evaporation of a DCM/pentane mixture (35 mg, 65%). **12a**: ^{1}H NMR δ: 9.54 (2H, d, *J* 5.1, β H), 8.68 (2H, d, *J* 5.1, β H), 8.48 (2H, d, *J* 4.9, β H), 8.40 (2H, d, *J* 4.9, β H), 7.86–7.84 (6H, m, phenyl H), 7.63–7.56 (9H, m, phenyl H), 1.71 (9H, s, CH_3); *m/z* (HR-ESI) 745.1833 ($[M+Na]^+$, $C_{43}H_{32}N_6NaNiO_2$ calcd 745.1838); ν_{max} (cm^{-1}) 1740 (CO); UV/vis: λ_{max}/nm ($\varepsilon/10^3$ M^{-1} cm^{-1}) 446 (200.8), 616 (25.3); Found: C, 70.72; H, 4.69; N, 11.11%; (Calcd C, 70.81; H, 4.06; N, 12.09). **13a**: ^{1}H NMR (CD_2Cl_2) δ: 9.34 (2H, d, *J* 4.9, β H), 8.64 (2H, d, *J* 5.0, β H), 8.56 (2H, d, *J* 5.0, β H), 8.54 (2H, d, *J* 5.0, β H), 7.93–7.88 (6H, m, phenyl H), 7.67 (1H, br s, amine N H) 7.65–7.59 (9H, m, phenyl H), 7.25 (1H, br s, amide N H), 1.45 (9H, s, CH_3), amine and amide N H peaks assigned using D_2O exchange experiments; *m/z* (HR-ESI) 747.1985 ($[M+Na]^+$, $C_{43}H_{34}N_6NaNiO_2$ calcd 747.1994); UV/vis: λ_{max}/nm ($\varepsilon/10^3$ M^{-1} cm^{-1}) 422 (202), 489 (10.4), 535 (12.6) 576 sh (3.8).

*4.2.7. 5-(Ethoxycarbonylazo)-10,15,20-triphenylporphyrinatonickel(II) (**12b**).* NiTriPPBr (**Ni5**, 20.0 mg, 0.0297 mmol), ethyl carbazate (10 equiv, 30.9 mg, 0.297 mmol), $Pd(OAc)_2$ (0.5 mg, 0.002 mmol), *rac*-BINAP (3.7 mg, 0.0059 mmol), Cs_2CO_3 (68.6 mg, 0.211 mmol) and dry THF (5 cm^3) were stirred for 22 h at 68 °C. The quenched reaction mixture was allowed to stir at room temperature, open to air, overnight. The product was purified using column chromatography (DCM). The resulting product **12b** was bright green (14 mg, 67% crude yield) and resisted recrystallisation. ^{1}H NMR showed that the sample was not pure enough for elemental analysis. ^{1}H NMR δ: 9.36 (2H, d, *J* 5.1, β H), 8.75 (2H, d, *J* 5.1, β H), 8.54 (2H, d, *J* 4.9, β H), 8.46 (2H, d, *J* 5.1, β H), 7.94–7.92 (6H, m, phenyl H), 7.71–7.65 (9H, m, phenyl H), 4.68 (2H, q, *J* 7.1, CH_2), 1.60 (3H, t, *J* 7.1, CH_3); *m/z* (LSIMS) 694.1650 (M^+, $C_{41}H_{28}N_6NiO_2$ calcd 694.1627); UV/vis: λ_{max}/nm 449, 621.

*4.2.8. N,N′-Bis(ethoxycarbonylamino)-5,15-diimino-10,20-diphenylporphodimethenatozinc(II) (**Zn8b**).* $ZnDPPBr_2$ (**Zn10**, 20.0 mg, 0.0293 mmol), ethyl carbazate (10 equiv, 30.5 mg, 0.293 mmol), $Pd(OAc)_2$ (0.5 mg, 0.002 mmol), *rac*-BINAP (3.6 mg, 0.0059 mmol), Cs_2CO_3 (67.7 mg, 0.208 mmol) and dry THF (5 cm^3) were stirred at 68 °C for 17.5 h. The product was purified by column chromatography [DCM then DCM/MeOH (100:1)], and the resulting red product **Zn8b** was recrystallised from DCM/pentane (17 mg, 82%). ^{1}H NMR δ: 9.07 (2H, br s, N H), 7.50–7.45 (10H, m, phenyl H), 7.25 (2H, *β H*, found from COSY and NOESY experiments), 6.88 (2H, d, *J* 3.9, β H), 6.77 (2H, d, *J* 4.4, β H), 6.67 (2H, d, *J* 3.9, β H), 4.27 (4H, q, *J* 7.1, CH_2), 1.31 (6H, t, *J* 7.2, CH_3); *m/z* (MALDI-TOF-MS) 727.1553

([M+H]$^+$, $C_{38}H_{31}N_8O_4Zn$ calcd 727.1760); ν_{max} (cm^{-1}) 3330 (NH), 1730 (CO); UV/vis: λ_{max}/nm ($\varepsilon/10^3$ M^{-1} cm^{-1}) 328 (35.8), 415 (36.7), 437 (53.4), 552 (33.3). Crystals of [Zn8b(pyridine)]·dioxane·$2H_2O$ suitable for X-ray structure determination were grown by the slow diffusion of water into a solution of **Zn8b** in dioxane and pyridine.

*4.2.9. N,N′-Bis(tert-butoxycarbonylamino)-5,15-diimino-10,20-diphenylporphodimethene (**$H_2$8a**).* H_2DPPBr (**$H_2$5**, 22.0 mg, 0.0407 mmol), *tert*-butyl carbazate (10 equiv, 53.9 mg, 0.407 mmol), $Pd(OAc)_2$ (0.6 mg, 0.003 mmol), *rac*-BINAP (5.0 mg, 0.0081 mmol), Cs_2CO_3 (94.1 mg, 0.289 mmol) and dry THF (6.5 cm^3) were stirred for 14.5 h at 68 °C. The mixture was purified using column chromatography [DCM then DCM/MeOH (100:1)]. The orange product **$H_2$8a** eluted upon the addition of MeOH and was purified from hot/cold MeOH/H_2O recrystallisation (8.8 mg, 37%). ^{1}H NMR δ: 12.42 (2H, br s, inner NH), 9.01 (2H, br s, NH), 7.50–7.45 (10H, m, phenyl H), 7.25 (2H, d, *J* 4.7, β H), 6.85 (2H, br dd, β H), 6.77 (2H, d, *J* 4.7, β H), 6.44 (2H, br dd, β H), 1.55 (18H, s, CH_3); *m*/*z* (ESI) 721.3260 ([M+H]$^+$, $C_{42}H_{41}N_8O_4$ calcd 721.3251); ν_{max} (cm^{-1}) 3330 (NH), 1720 (CO); UV/vis: λ_{max}/nm ($\varepsilon/10^3$ M^{-1} cm^{-1}) 316 (35.7), 394 (38.2), 489 (32.2).

*4.2.10. N,N′-Bis(ethoxycarbonylamino)-5,15-diimino-10,20-diphenylporphodimethene (**$H_2$8b**).* H_2DPPBr$_2$ (**$H_2$5**, 20.0 mg, 0.0322 mmol), ethyl carbazate (10 equiv, 33.5 mg, 0.322 mmol), $Pd(OAc)_2$ (0.5 mg, 0.002 mmol), *rac*-BINAP (4.0 mg, 0.0064 mmol), Cs_2CO_3 (74.4 mg, 0.228 mmol) and dry THF (5 cm^3) were stirred at 68 °C for 20 h. The product was purified by column chromatography [DCM/TEA (200:1) then DCM/MeOH/TEA (200:1:1), two columns], yielding impure dark orange product **$H_2$8b** (13 mg, 54%). ^{1}H NMR δ: 12.47 (2H, br s, inner N H), 9.08 (2H, br s, N H), 7.50–7.45 (10H, m, phenyl *H*), 6.85 (2H, d, *J* 4.9, *β H*), 6.84 (2H, dd, *J* 4.0, 1.8, *β H*), 6.55 (2H, d, *J* 4.9, β H), 6.54 (2H, dd, *J* 4.0, 1.8, β H), 4.34 (4H, q, *J* 7.1, CH_2), 1.35 (6H, t, *J* 7.1, CH_3); *m*/*z* (MALDI-TOF-MS) 665.2613 ([M+H]$^+$, $C_{38}H_{33}N_8O_4$ calcd 665.2625); ν_{max} (cm^{-1}) 3330 (NH), 1720 (CO).

*4.2.11. 5-(tert-Butoxycarbonylazo)-10,20-bis(3,5-di-tert-butylphenyl)-15-phenylporphyrin (**15**).* H_2DAPPBr (**14**, 50 mg, 0.059 mmol), *tert*-butyl carbazate (10 equiv, 63.1 mg, 0.590 mmol), $Pd(dppe)_2$ (7 mol %, 3.8 mg, 0.004), Cs_2CO_3 (7.1 equiv, 137.4 mg, 0.420 mmol) and dry THF (10 cm^3) were stirred at 68 °C for 23 h and the major product seen by TLC was the green azocarboxylate **15**. This product was separated using column chromatography [DCM]. Two other compounds were isolated by a second column [toluene: ethyl acetate 1%], these being blue **16** and violet **17**. The compounds were recrystallised from dioxane/water (**15**: 15.3 mg, 29% yield, **16**: 5.8 mg, **17**: 1.0 mg). **15**: ^{1}H NMR δ: 9.84 (2H, d, *J* 4.9 Hz, β H), 8.88 (2H, d, *J* 4.9 Hz, β H), 8.65 (4H, br s, β H), 8.14 (2H, d, phenyl H), 8.01 (4H, m, phenyl H), 7.80 (2H, m, phenyl H), 7.73 (3H, m, phenyl H), 1.55 (9H, s, Bu^t H), 1.53 (36H, s, ^{t}Bu H), −1.29 (2H, s, inner H); *m*/*z* (ESIMS) 891.5314 ([M+H]$^+$, $C_{59}H_{67}N_6O_2$ calcd 891.5326); UV/vis: λ_{max}/nm ($\varepsilon/10^3$ M^{-1} cm^{-1}) 435 (65.1), 602 (8.7), 677 (5.2), 824 (2.4). **16**: ^{1}H NMR δ: 12.54 (1H, s, N H), 10.51 (1H, s, N H), 10.28 (1H, s, N H), 8.45 (1H, s, N H), 7.73 (2H, d, *o*-Ar H), 7.65 (1H, t, *p*-Ar H), 7.54 (1H, t, *p*-Ar H), 7.45–7.37 (5H, m, Ph H), 7.34 (2H, d, *o*-Ar H), 6.92 (1H, dd, β H), 6.86 (1H, d, *J* 5.5 Hz, β H), 6.78 (1H, d, *J* 4.5 Hz, β H), 6.71 (1H, dd, β H), 6.52 (1H, d, *J* 4.5 Hz, β H), 6.51 (1H, d, *J* 4.5 Hz, β H), 6.29 (1H, d, *J* 4.5 Hz, β H), 6.03 (1H, br d, *J* 5.5 Hz, β H), 1.46 (9H, s, ^{t}Bu H), 1.36 (18H, s, ^{t}Bu H), 1.35 (18H, s, ^{t}Bu H); UV/vis: λ_{max}/nm (intensity ratio) 370 (1.9), 580 (1.0). **16** and **17**: *m*/*z* (ESIMS) **16**: 925.5382, **17**: 925.5385 ([M+H+CH_3OH]$^+$, $C_{60}H_{73}N_6O_3$ calcd 925.5744).

4.3. Redox reactions of the coupling products

*4.3.1. The oxidation of 5-[2-(ethoxycarbonyl)hydrazo]-10,15,20-triphenylporphyrinatonickel(II) (**13b**).* Carbazate porphyrin **13b** (32 mg, 0.044 mmol) was dissolved in DCM (1.5 cm^3) and DDQ (1.1 equiv, 11 mg, 0.0049 mmol) was added. The mixture was shaken and then passed through a short column [DCM/*n*-hexane (1:1)]. The bright green azocarboxylate **12b** was recrystallised by the evaporation of a mixture of DCM/pentane, to give a dark green powder (30 mg, 95% from two crops), having ^{1}H NMR data identical to those of the product described in Section 4.2.6.

*4.3.2. The reduction of 5-(tert-butoxycarbonylazo)-10,15,20-triphenylporphyrinatonickel(II) (**12a**).* Azocarboxylate porphyrin **12a** (26 mg, 0.035 mmol) was dissolved in THF/MeOH (4 cm^3/8 drops) and $NaBH_4$ (10 equiv, 13 mg, 0.35 mmol) was added. The mixture was stirred at room temperature for 40 min, after which the only significant product was the carbazate porphyrin **13a**. The mixture was then refluxed for 20 h and the major product was NiTriPP, which was recrystallised from DCM/pentane (10 mg, 48%). A small amount of the aminoporphyrin **Ni1b** was also isolated, and was recrystallised by the evaporation of a mixture of DCM/MeOH (1 mg, 5%). Both products were identified by comparison of their ^{1}H NMR spectra with those of authentic samples.[18,42]

*4.3.3. The oxidation of N,N′-bis(tert-butoxycarbonylamino)-5,15-diimino-10,20-diphenylporphodimethenatonickel(II) (**Ni8a**) to give 5,15-bis(t-butoxycarbonylazo)-10,20-diphenylporphyrinatonickel(II) (**19a**).* The DIPD (**Ni8a** 28 mg, 0.035 mmol) was dissolved in DCM (4 cm^3), DDQ (2.1 equiv, 17 mg, 0.075 mmol) was added and the mixture was shaken briefly. The mixture was separated using column chromatography (DCM) to give the bright green bis(azocarboxylate) **19a** (21 mg, 77%), which was recrystallised from DCM/pentane to give a dark green powder (12 mg, 36%). ^{1}H NMR δ: 9.50 (4H, d, *J* 5.0, β H), 8.69 (4H, d, *J* 5.0, β *H*), 7.93–7.91 (4H, m, phenyl H), 7.73–7.67 (6H, m, phenyl H), 1.79 (18H, s, CH_3); *m*/*z* (LSIMS) 774.2223 (M^+, $C_{42}H_{36}N_8NiO_4$ calcd 774.2213); ν_{max} (cm^{-1}) 1740 (CO); UV/vis: λ_{max} ($\varepsilon/10^3$ M^{-1} cm^{-1}) 321 (22.8), 449 (128), 645 (21.5).

*4.3.4. The oxidation of N,N′-bis(ethoxycarbonylamino)-5,15-diimino-10,20-diphenylporphodimethenatonickel(II) (**Ni8b**) to give 5,15-bis(ethoxycarbonylazo)-10,20-diphenylporphrinatonickel(II) (**19b**).* The DIPD **Ni8b** (15 mg, 0.021 mmol) was dissolved in DCM (2 cm^3), DDQ (2.1 equiv, 10 mg, 0.045 mmol) was added and the mixture was shaken briefly. The mixture was separated using column chromatography (DCM) to give the bright green bis(azocarboxylate) **19b** (13 mg, 86%), which was recrystallised from DCM/pentane to give the fluffy blue product (11 mg, 71%). ^{1}H NMR δ: 9.46 (4H, d, *J* 5.0, β H), 8.63 (4H, d, *J* 5.0, β H), 7.88–7.86 (4H, m, phenyl H), 7.71–7.64 (6H, m, phenyl H), 4.69 (4H, q, *J* 7.1, CH_2), 1.59 (6H, t, *J* 7.1, CH_3); *m*/*z* (MALDI-TOF-MS) 719.12 ([M+H$^+$], $C_{38}H_{29}N_8NiO_4$ calcd 719.17); ν_{max} (cm^{-1}) 1741 (CO); UV/vis: λ_{max} ($\varepsilon/10^3$ M^{-1} cm^{-1}) 330 (24.7), 452 (132), 653 (23.6); Found: C, 63.43; H, 4.04; N, 15.50%; (Calcd C, 63.45; H, 3.92; N, 15.58).

*4.3.5. The reduction of 5,15-bis(ethoxycarbonylazo)-10,20-diphenylporphrinatonickel(II) (**19b**).* Bis(azocarboxylate) **19b** (5.0 mg, 0.0070 mmol) was dissolved in THF/MeOH (2 cm^3/4 drops) and $NaBH_4$ (10 equiv, 2.6 mg, 0.070 mmol) was added. The mixture was stirred at room temperature for 1 day and then refluxed for 23 h. The mixture was purified by column chromatography [DCM/EtOAc (9:1) then (1:1)] to give DIPD **Ni8b** (3.0 mg, 59%), which was identified by comparison of its ^{1}H NMR spectrum with that of an authentic sample prepared as in Section 4.2.4.

4.4. Crystal structure determination of [Zn8b(pyridine)]·dioxane·$2H_2O$

Data for [**Zn8b**(pyridine)]·dioxane·$2H_2O$ were collected at approximately 150 K using double diamond monochromated synchrotron radiation (0.48595 Å) using ω and ψ scans at the

ChemMatCARS beamline at the Advanced Photon Source. Data integration and reduction were undertaken with SAINT and XPREP.[42a] Subsequent computations were carried out using the WinGX-32 graphical user interface.[42b] Structures were solved by direct methods using SIR97.[42c] Data were refined and extended with SHELXL-2013.[42d] Non-hydrogen atoms were refined anisotropically. The complex has crystallographic twofold symmetry (the twofold axis is coincident with the Zn–$N_{pyridine}$ bond and the dioxane molecule has crystallographic inversion symmetry). The water molecules occupy general positions in the unit cell. Carbon-bound hydrogen atoms were included in idealised positions and refined using a riding model. The nitrogen-bound hydrogen atom H(3) was located in the difference map and refined without restraints. As oxygen bound hydrogen atoms (associated with the water of crystallization) could not be located in the difference Fourier map they were not modelled.

Crystal data and refinement details for [**Zn8b**(pyridine)]·dioxane·$2H_2O$: $C_{47}H_{47}N_9O_8Zn$, M=931.10, monoclinic, $P2/c$, a=12.4001(8) Å, b=12.8989(8) Å, c=13.5031(9) Å, β=96.163(3)°, V=2147.3(2) Å^3, D_c=1.440 g cm^{-3}, Z=2, crystal size 0.090×0.080×0.015 mm, purple plate, 150(2) K, λ(Mo-Kα)=0.71073, $2\theta_{max}$=44.9°, hkl range −19 to 19, −20 to 18, −21 to 19, N=33,020, N_{ind}=7943 (R_{merge}=0.060), N_{obs}=5558 ($I>2\sigma(I)$), N_{var}=299, residuals $R1(F, 2\sigma)$=0.051, $wR2(F^2$, all)=0.125, GoF(all)=1.351, $\Delta\rho_{min,max}$=−0.79, 1.15 e Å^{-3}. The refinement residuals are defined as $R1=\Sigma||F_o|-|F_c||/\Sigma|F_o|$ for $F_o>2\sigma(F_o)$ and $wR2=\{\Sigma[w(F_o^2-F_c^2)^2]/\Sigma[w(F_c^2)^2]\}^{1/2}$ where $w=1/[\sigma^2(F_o^2)+(0.04P)^2+0.5P]$, $P=(F_o^2+2F_c^2)/3$. The CIF file has been deposited with the Cambridge Structural Database (CCDC reference number 953602) and can be obtained free of charge via www.ccdc.cam.ac.uk/conts/retrieving.html (or from the Cambridge Crystallographic Data Centre, 12 Union Road, Cambridge CB2 1EZ, UK; fax: (+44) 1223-336-033; or deposit@ccdc.cam.ac.uk).

4.5. Computational methods

The initial geometries of the porphyrin **19c** and porphodimethene **Ni8c** were first calculated at the semi-empirical level using the PM3 method. The geometry was then further optimised by performing a restricted closed-shell calculation with Gaussian 09[43] using the DFT model with Becke's three-parameter hybrid functional, Lee, Yang and Parr's correction for correlation interactions and a 6-31G(d,p) basis set.[44] Time-dependent DFT calculations were subsequently performed on the resulting optimised geometries at the same level. The electron density difference map of the HOMO to LUMO transition of **19c** was constructed with the aid of the Gaussum program[43] and displayed using an isovalue of 0.0004 e/Å^3.

Acknowledgements

We thank Queensland University of Technology (QUT) for a post-graduate scholarship for L.E., the Australian Research Council for financial assistance (DP0663774), and the High Performance Computing team, Queensland University of Technology (QUT) for their support of the Gaussian 09 program. Use of the ChemMatCARS Sector 15 at the Advanced Photon Source was supported by the Australian Synchrotron Research Program, which is funded by the Commonwealth of Australia under the Major National Research Facilities Program. ChemMatCARS Sector 15 is also supported by the National Science Foundation/Department of Energy. The Advanced Photon Source is supported by the U.S. Department of Energy, Basic Energy Sciences.

Supplementary data

These data include partial ^{1}H NMR spectra for all previously unreported compounds, calculated orbital surfaces for compounds **Ni8c**, and tables of TD-DFT calculated excited states for **Ni8c**. The optimised geometries are provided as .mol files. Supplementary data related to this article can be found at http://dx.doi.org/10.1016/j.tet.2013.11.006.

References and notes

1. Screen, T. E. O.; Blake, I. M.; Rees, L. H.; Clegg, W.; Borwick, S. J.; Anderson, H. L. *J. Chem. Soc., Perkin Trans. 1* **2002**, 320.
2. Esdaile, L. J.; Jensen, P.; McMurtrie, J. C.; Arnold, D. P. *Angew. Chem., Int. Ed.* **2007**, *46*, 2090.
3. Bašić, B.; McMurtrie, J. C.; Arnold, D. P. *J. Porphyrins Phthalocyanines* **2010**, *14*, 482.
4. Bašić, B.; McMurtrie, J. C.; Arnold, D. P. *Eur. J. Org. Chem.* **2010**, 4329.
5. Shen, D. M.; Lin, C.; Chen, X. G.; Chen, Q. Y. *Synlett* **2009**, 945.
6. Smith, M. J. D. Phil. Thesis, University of Oxford, 2004.
7. Wang, Z.; Skerlj, R. T.; Bridger, G. J. *Tetrahedron Lett.* **1999**, *40*, 3543.
8. Lim, Y. K.; Lee, K. S.; Cho, C. G. *Org. Lett.* **2003**, *5*, 979.
9. Kim, K.-Y.; Shin, J.-T.; Lee, K.-S.; Cho, C.-G. *Tetrahedron Lett.* **2004**, *45*, 117.
10. Takanami, T.; Hayashi, M.; Hino, F.; Suda, K. *Tetrahedron Lett.* **2003**, *44*, 7353.
11. Chen, Y.; Gao, G.-Y.; Zhang, X. P. *Tetrahedron Lett.* **2005**, *46*, 4965; (b) Gao, G.-Y.; Chen, Y.; Zhang, P. *Org. Lett.* **2004**, *6*, 1837; (c) Chen, Y.; Zhang, X. P. *J. Org. Chem.* **2003**, *68*, 4432.
12. (a) Akita, M.; Hiroto, S.; Shinokubu, H. *Angew. Chem., Int. Ed.* **2012**, *51*, 2894; (b) Ladomenou, K.; Lazarides, T.; Panda, M. K.; Charalambidis, G.; Daphnomili, D.; Coutsolelos, A. G. *Inorg. Chem.* **2012**, *51*, 10548; (c) Abada, Z.; Ferrié, L.; Akagah, B.; Lormier, A. T.; Figadère, B. *Tetrahedron Lett.* **2012**, *53*, 6961; (d) Pereira, A. M. V. M.; Neves, M. G. P. M. S.; Cavaleiro, J. A. S.; Jeandon, C.; Gisselbrecht, J.-P.; Choua, S.; Ruppert, R. *Org. Lett.* **2011**, *13*, 4742; (e) Sakamoto, R.; Nishikawa, M.; Yamamura, T.; Kume, S.; Nishihara, H. *Chem. Commun.* **2010**, 2028; (f) Shen, D.-M.; Liu, C.; Chen, X.-G.; Chen, Q.-Y. *J. Org. Chem.* **2009**, *74*, 206; (g) Liu, C.; Shen, D.-M.; Chen, Q.-Y. *J. Org. Chem.* **2007**, *72*, 2732.
13. (a) Warnan, J.; Favereau, L.; Meslin, F.; Severac, M.; Blart, E.; Pellegrin, Y.; Jacquemin, D.; Odobel, F. *ChemSusChem* **2012**, *5*, 1568; (b) Liu, Y.; Lin, H.; Dy, J. T.; Tamaki, K.; Nakazaki, J.; Nakayama, D.; Uchida, S.; Kubo, T.; Segawa, H. *Chem. Commun.* **2011**, 4010; (c) Lee, C.-W.; Lu, H.-P.; Reddy, N. M.; Lee, H.-W.; Diau, E. W.-G.; Yeh, C.-Y. *Dyes Pigm.* **2011**, *91*, 317; (d) Mathew, S.; Iijima, H.; Toude, Y.; Umeyama, T.; Matano, Y.; Ito, S.; Tkachenko, N. V.; Lemmetyinen, H.; Imahori, H. *J. Phys. Chem. C* **2011**, *115*, 14415; (e) Imahori, H.; Matsubara, Y.; Iijima, H.; Umeyama, T.; Matano, Y.; Ito, S.; Niemi, K.; Tkachenko, N. V.; Lemmetyinen, H. *J. Phys. Chem. C* **2010**, *114*, 10656; (f) Lee, C.-W.; Lu, H.-P.; Lan, C.-M.; Huang, Y.-L.; Liang, Y.-R.; Yen, W.-N.; Liu, Y.-C.; Lin, Y.-S.; Diau, E. W.-G.; Yeh, C.-Y. *Chem.—Eur. J.* **2009**, *15*, 1403.
14. Esdaile, L. J.; McMurtrie, J. C.; Turner, P.; Arnold, D. P. *Tetrahedron Lett.* **2005**, *46*, 6931.
15. Yamashita, K.-i.; Takeuichi, S.; Asano, M. S.; Sugiura, K.-i. *Book of Abstracts*. International Conference on Porphyrins and Phthalocyanines; Society of Porphyrins and Phthalocyanines: Jeju, South Korea, Jul 1–6, 2012; p 583.
16. Kwong, F. Y.; Klapars, A.; Buchwald, S. L. *Org. Lett.* **2002**, *4*, 581.
17. (a) Yamashita, K.-i.; Kataoka, K. .; Asano, M. S.; Sugiura, K.-i. *Org. Lett.* **2012**, *14*, 190; (b) Balaban, M. C.; Gillot-Chappaz, C.; Canard, G.; Fuhr, O.; Roussel, C.; Balaban, T. S. *Tetrahedron* **2009**, *65*, 3733.
18. Esdaile, L. J.; Senge, M. O.; Arnold, D. P. *Chem. Commun.* **2006**, 4192.
19. Harper, S. R.; Arnold, D. P. Unpublished results.
20. Bašić, B. Ph.D. Thesis, Queensland University of Technology, 2010.
21. Blake, I. M.; Anderson, H. L.; Beljonne, D.; Bredas, J.-L.; Clegg, W. *J. Am. Chem. Soc.* **1998**, *120*, 10764.
22. Senge, M. O.; Smith, K. M. *Z. Naturforsch., B: Chem. Sci.* **1993**, *48*, 991.
23. Kamo, M.; Tsuda, A.; Nakamura, Y.; Aratani, N.; Furukawa, K.; Kato, T.; Osuka, A. *Org. Lett.* **2003**, *5*, 2079.
24. Senge, M. O. In *The Porphyrin Handbook*; Kadish, K. M., Smith, K. M., Guilard, R., Eds.; Academic: London, 2000; Vol. 10, pp 1–218.
25. Arnold, D. P.; Bott, R. C.; Eldridge, H.; Elms, F. M.; Smith, G.; Zojaji, M. *Aust. J. Chem.* **1997**, *50*, 495.
26. Sprutta, N.; Rath, S. P.; Olmstead, M. M.; Balch, A. L. *Inorg. Chem.* **2005**, *44*, 1452.
27. Fuhrhop, J.-H. *J. Chem. Soc., Chem. Commun.* **1970**, 781.
28. Barnett, G. H.; Evans, B.; Smith, K. M. *Tetrahedron* **1975**, *31*, 2711.
29. Smith, M. J.; Clegg, W.; Nguyen, K. A.; Rogers, J. E.; Pachter, R.; Fleitz, P. A.; Anderson, H. L. *Chem. Commun.* **2005**, 2433.
30. Balch, A. L.; Mazzanti, M.; Olmstead, M. M. *Inorg. Chem.* **1993**, *32*, 4737.
31. Blake, I. M.; Rees, L. H.; Claridge, T. D. W.; Anderson, H. L. *Angew. Chem., Int. Ed.* **2000**, *39*, 1818.
32. McCallien, D. W. J.; Sanders, J. K. M. *J. Am. Chem. Soc.* **1995**, *117*, 6611.
33. Fuhrhop, J.-H.; Baumgartner, E.; Bauer, H. *J. Am. Chem. Soc.* **1981**, *103*, 5854.
34. Stillman, M. J. In *Handbook of Porphyrin Science*; Kadish, K. M., Smith, K. M., Guilard, R., Eds.; World Scientific: Singapore, 2010; Vol. 14, pp 461–524.
35. Lee, C.-H.; Roznyatovskiy, V.; Hong, S.-J.; Sessler, J. L. In *Handbook of Porphyrin Science*; Kadish, K. M., Smith, K. M., Guilard, R., Eds.; World Scientific: Singapore, 2010; Vol. 13, pp 197–252.
36. Schill, F.; Arnold, D.P. Unpublished results.
37. Bašić, B.; Locos, O. B.; Rintoul, L.; Kan, J.; Jiang, J.; Arnold, D. P. In preparation.
38. Manka, J. S.; Lawrence, D. S. *Tetrahedron Lett.* **1989**, *30*, 6989.
39. DiMagno, S. G.; Lin, V. S. Y.; Therien, M. J. *J. Org. Chem.* **1993**, *58*, 5983.
40. Senge, M. O.; Feng, X. *J. Chem. Soc., Perkin Trans. 1* **2000**, 3615.

41. Hartnell, R. D.; Edwards, A. J.; Arnold, D. R. *J. Porphyrins Phthalocyanines* **2002**, *6*, 695.
42. (a) Bruker. *SMART, SAINT and XPREP*; Bruker, Analytical X-ray Instruments: Madison, Wisconsin, USA, 1995; (b) Farrugia, L. J. *J. Appl. Crystallogr.* **1999**, *32*, 837; (c) Altomare, A.; Burla, M. C.; Camalli, M.; Cascarano, G. L.; Giocavazzo, C.; Guagliardi, A.; Moliterni, A. G. C.; Polidori, G.; Spagna, S. *J. Appl. Crystallogr.* **1999**, *32*, 115; (d) Sheldrick, G. M. *Acta Crystallogr.* **2008**, *D64*, 112.
43. Frisch, M. J.; Trucks, G. W.; Schlegel, H. B.; Scuseria, G. E.; Robb, M. A.; Cheeseman, J. R.; Scalmani, G.; Barone, V.; Mennucci, B.; Petersson, G. A.; Nakatsuji, H.; Caricato, M.; Li, X.; Hratchian, H. P.; Izmaylov, A. F.; Bloino, J.; Zheng, G.; Sonnenberg, J. L.; Hada, M.; Ehara, M.; Toyota, K.; Fukuda, R.; Hasegawa, J.; Ishida, M.; Nakajima, T.; Honda, Y.; Kitao, O.; Nakai, H.; Vreven, T.; Montgomery, J. A., Jr.; Peralta, J. E.; Ogliaro, F.; Bearpark, M.; Heyd, J. J.; Brothers, E.; Kudin, K. N.; Staroverov, V. N.; Kobayashi, R.; Normand, J.; Raghavachari, K.; Rendell, A.; Burant, J. C.; Iyengar, S. S.; Tomasi, J.; Cossi, M.; Rega, N.; Millam, J. M.; Klene, M.; Knox, J. E.; Cross, J. B.; Bakken, V.; Adamo, C.; Jaramillo, J.; Gomperts, R.; Stratmann, R. E.; Yazyev, O.; Austin, A. J.; Cammi, R.; Pomelli, C.; Ochterski, J. W.; Martin, R. L.; Morokuma, K.; Zakrzewski, V. G.; Voth, G. A.; Salvador, P.; Dannenberg, J. J.; Dapprich, S.; Daniels, A. D.; Farkas, Ö.; Foresman, J. B.; Ortiz, J. V.; Cioslowski, J.; Fox, D. J. *Gaussian 09, Revision A.1*; Gaussian: Wallingford CT, 2009.
44. (a) Becke, A. D. *J. Chem. Phys.* **1993**, *98*, 5648; (b) Lee, C.; Yang, W.; Parr, R. G. *Phys. Rev. B* **1988**, *37*, 785; (c) Vosko, S. H.; Wilk, L.; Nusair, M. *Can. J. Phys.* **1980**, *58*, 1200; (d) Stephens, P. J.; Devlin, F. J.; Chabalowski, C. F.; Frisch, M. J. *J. Phys. Chem.* **1994**, *98*, 11623.